The exocyst complex and intracellular vesicles mediate soluble protein trafficking to the primary cilium

Niedziółka SM[1,2], Datta S[1], Uśpieński T[1,2], Baran B[1,2], Skarżyńska W[1], Humke EW[3,4], Rohatgi R[3,5], Niewiadomski P[1,*]

[1] Centre of New Technologies, University of Warsaw, Warsaw, Poland
[2] Faculty of Biology, University of Warsaw, Warsaw, Poland
[3] Department of Medicine, Stanford University School of Medicine, Stanford, CA, USA
[4] Current address: IGM Biosciences, Inc., Mountain View, CA, USA
[5] Department of Biochemistry, Stanford University School of Medicine, Stanford, CA, USA
[*] Correspondence: p.niewiadomski@cent.uw.edu.pl

Abstract

The efficient transport of proteins into the primary cilium is a crucial step for many signaling pathways. Dysfunction of this process can lead to the disruption of signaling cascades or cilium assembly, resulting in developmental disorders and cancer. Previous studies on the protein delivery to the cilium were mostly focused on the membrane-embedded receptors. In contrast, how soluble proteins are delivered into the cilium is poorly understood. In our work, we identify the exocyst complex as a key player in the ciliary trafficking of soluble Gli transcription factors. In line with the known function of the exocyst in intracellular vesicle transport, we demonstrate that soluble proteins, including Gli2/3 and Lkb1, can use the endosome recycling machinery for their delivery to the primary cilium. Finally, we identify GTPases: Rab14, Rab18, Rab23, and Arf4 that are involved in vesicle-mediated Gli protein ciliary trafficking. Our data pave the way for a better understanding of ciliary transport and uncover novel transport mechanisms inside the cell.

Introduction

Hedgehog (Hh) signaling is essential for embryonic patterning and organ morphogenesis[1]. Malfunctions of this pathway can lead to developmental disorders and cancer. The expression of Hh target genes is controlled by Gli transcription factors: Gli1 which acts as an activator, and Gli2/Gli3, which display both activator and repressor functions[2].

Processing of Gli transcription factors to activator and repressor forms requires their efficient transport to the primary cilium, which integrates proteins necessary to a variety of Gli modifications[3–8]. Cilia are indispensable for the transduction of the Hh signal and the translocation of Gli activators into the nucleus[9]. In humans, defects in the ciliary function and the trafficking of ciliary proteins often result in developmental defects associated with the dysfunction of the Hh/Gli cascade.

Gli proteins are large and slowly diffusing proteins, so it is puzzling how they accumulate at the cilium within a mere few minutes upon signal reception[10]. This accumulation is a result of a three-step process: (1) targeted transport to the cilium base, (2) gated entry through a diffusion barrier, and (3) active trafficking along the cilium. The mechanisms of Gli transition across the diffusion barrier and the model of transport from the base to the tip are relatively

well-described[11–13]. Specifically, inside the cilium the Gli proteins appear to utilize the conserved intraflagellar transport (IFT) system for the delivery from the base of the cilium to the tip and back to the base[10,14–18]. At the base of the cilium, Gli proteins must pass the diffusion barrier reminiscent of the nuclear pore with the help of some of the same molecular players as those involved in nucleocytoplasmic shuttling: Ran, importins, and exportins[12,19,20]. However, it is still unclear how Gli proteins are delivered from the cytoplasm to the cilium base in the first place.

Most previous studies on protein delivery to the ciliary base were focused on membrane proteins. Three different transport routes have been described for their delivery from the Golgi complex to the primary cilium[21]. Some ciliary proteins first reach the plasma membrane and then move to the ciliary membrane by lateral transport[22]. Others reach the base of the cilium using regulated vesicular transport, either directly or through the recycling trafficking pathway[23].

The process of protein trafficking to the primary cilium is supported by many players involved in endocytosis and the vesicle transport machinery[24–26]. Prominent among them are small GTPases, which act as molecular switches that allow for the guidance of their associated vesicles[27–29]. In addition to GTPases, the protein ciliary trafficking depends on several multiprotein complexes, such as the BBsome[30,31] and the exocyst[32,33]. The exocyst, in particular, is a conserved protein complex that mediates the tethering of secretory vesicles to the plasma membrane[34]. Many protein trafficking routes depend on the exocyst, including those for protein delivery to the cell junctions and protein endocytosis and recycling[35,36]. The transport function of the exocyst relies on its interaction with membrane phospholipids [37,38], polarity proteins[39,40] and small GTPases[40–43]. Importantly, the exocyst interacts with the ciliary transport machinery, and has been implicated in the transport of transmembrane proteins necessary for ciliogenesis and signaling[23,42,44–47], but its role in the trafficking of soluble ciliary proteins has not been demonstrated.

In our quest to identify the molecular machinery that delivers Gli proteins to the cilium base, we performed a proteomic analysis of Gli3 interactors. Interestingly, among Gli3-binding proteins, we detected several exocyst subunits[34]. Loss-of-function assays show the dependence of Gli2 and Gli3 ciliary localization on the exocyst. Consistent with the role of this complex in vesicle trafficking, we show that Gli2 uses intracellular vesicles as trafficking vehicles. In addition, several small GTPases, including Rab14, Rab18, Rab23, and Arf4, regulate the ciliary transport of Gli2. Finally, we show that this vesicle-based transport machinery is used for the ciliary delivery of Lkb1, another soluble protein that concentrates at cilia. Our study uncovers a novel vesicle-dependent transport pathway for soluble ciliary proteins and sheds new light on the mechanisms of protein delivery to the cilium base.

Results

The exocyst complex interacts with Gli3

To identify proteins that help guide Gli proteins to the primary cilium, we immunoprecipitated proteins that interact with Gli3 in cells treated with the Smoothened (Smo) agonist SAG[48]. Cells were separated into "nuclear" and "cytoplasmic" fractions using hypotonic lysis and low-speed centrifugation, and each fraction was immunoprecipitated with anti-Gli3 antibodies. The eluates were separated using SDS-PAGE, and prominent bands were submitted for MS-based protein identification (Fig. 1A).

Mascot's search of the MS spectra yielded a total of 898 unique proteins. From this dataset, we selected 473 high confidence Gli3 interactors by rejecting proteins that are frequently found as IP/MS contaminants based on the CRAPome database[49]. In this dataset, we found well-known Gli interaction partners, such as SuFu, Kif7, and Xpo7[50–53]. The dataset was enriched for proteins involved in intraciliary and vesicle transport, chromatin remodeling, and DNA repair (Fig. 1B) and contained components of multi-subunit ciliary transport complexes, including the BBSome and the exocyst (Fig. 1C, Supplementary Table S1).

Because exocyst, a multi-subunit protein complex involved in vesicle transport and docking[54], had previously been implicated in the trafficking of proteins to primary cilia, we decided to focus on its components as potential mediators of the Gli proteins delivery to the cilium base. The exocyst has mostly been studied in the context of its binding to intracellular vesicles and the plasma membrane, but the subunits that were specifically enriched in the Gli3 interactome are positioned away from the putative lipid-binding surface of the complex, consistent with Gli3 being a soluble, rather than a lipid-embedded protein (Fig. 1D).

In agreement with the proteomic data, Gli3, as well as Gli2, co-immunoprecipitate with Sec5 (Fig. 2A). Moreover, Sec5 and Gli2 tightly colocalize in cells, as shown using the proximity ligation assay (Fig. 2B, Fig. S1). Similarly, overexpressed Sec3, Sec5, and Sec8 interact with the constitutively active Gli2 mutants Gli2(P1-6A) (Fig. 2C, D)[55]. We decided to use Gli2(P1-6A) in most experiments because it localizes to cilia in the absence of upstream activation, allowing us to study its trafficking independently of the transport of membrane proteins regulating endogenous Gli proteins, such as Smo and Ptch[56,57].

To identify the Gli2 domain responsible for interaction with the exocyst, we performed co-immunoprecipitation of Sec3/5/8 with the N-terminal domain of Gli2 and a construct lacking the N-terminus. The exocyst subunits interact with the N-terminus of Gli2 (HA-Gli2-N) but interact only weakly with Gli2(P1-6A)-ΔN (Fig. 2E, F).

Trafficking of Gli2 to cilia depends on the exocyst

Because the exocyst is required for the trafficking of some ciliary proteins, we hypothesized that the loss-of-function of the exocyst could impair Gli ciliary localization. To test this assertion, we knocked down individual exocyst subunits in cells expressing Gli2(P1-6A). Both shRNA- (Fig. 3A) and siRNA-mediated knockdown (Fig. 3B) of exocyst subunits resulted in a significant reduction of Gli2(P1-6A) ciliary localization in NIH/3T3 (Fig. 3C and D) and mIMCD3 cells (Fig. S2A). Similarly, the SAG-induced ciliary accumulation of endogenous Gli2 is reduced in NIH/3T3 cells with Sec3/5/8 knockdown (Fig. S2B)

117 Similarly, mislocalization of Sec5 using the mitochondrial trap[58] impairs the ciliary trafficking
118 of Gli2(P1-6A). We fused Sec5 with the mitochondrial protein Tom20 and mScarlet and co-
119 expressed the resulting Tom20-mScarlet-Sec5 construct with Gli2(P1-6A) (Fig. 4A). We
120 observed a reduced Gli2 ciliary level in cells overexpressing the Tom20-mScarlet-Sec5
121 mitochondrial trap, compared to those overexpressing two negative control constructs –
122 Tom20-mScarlet and mScarlet-Sec5 (Fig. 4B).

123 Finally, the exocyst inhibitor endosidin2[59] reduces Gli2(P1-6A) ciliary localization in the stable
124 cell line after just two hours of treatment (Fig. 4C).

125 Because the exocyst binds to Gli2 mostly via its N-terminal domain (Fig 2E, F), we suspected
126 that removing the N-terminus would impair Gli2 ciliary accumulation. Accordingly, we
127 observed a strong reduction of the Gli2(P1-6A)-ΔN mutant localization in the primary cilium
128 compared to the full-length protein (Fig. 4D).

129 Having demonstrated that the exocyst is required for the trafficking of Gli to cilia, we
130 wondered if the localization of the exocyst is affected by Hh pathway activation. Indeed, the
131 treatment with SAG increases the amount of Sec3 and Sec5 at the ciliary base (Fig. 4E).

132 Gli2 associates with intracellular vesicles

133 While the best-known role of the exocyst complex is the transport of vesicle-embedded
134 membrane proteins, our results suggest that soluble cytoplasmic Gli proteins may also use the
135 exocyst as a vehicle for intracellular trafficking. We, therefore, wondered if Gli proteins, like
136 membrane receptors, use vesicles for their transport into the cilium. To verify this hypothesis,
137 we used super-resolution AiryScan microscopy to image cells co-expressing HA-Gli2(P1-6A)
138 and EGFP-Sec5, and surprisingly, we observed Gli2 around Sec5-positive vesicle-like
139 structures. It suggests that Gli2 could accumulate on the surface of vesicles, where it could
140 interact directly with the exocyst (Fig. 5A).
141
142 We also looked at Gli2 localization by immunogold electron microscopy. In HEK293T cells
143 overexpressing EGFP-Gli2(P1-6A), we observed EGFP-positive clusters adjacent to membrane
144 vesicle-like structures (Fig. 5B).

145 To check if Gli-positive structures represent intracellular vesicles, we isolated vesicles using
146 cell fractionation. HA-Gli2(P1-6A), endogenous Gli3, and Sec5 co-fractionated with the
147 endosome marker EEA1 in the endosomal fraction. ERK was used as the cytoplasmic control
148 marker. The total abundance of proteins in fractions we showed by silver staining (Fig. 5C).

149 The most likely explanation for our results is that Gli proteins are transported on the surface
150 of vesicles towards the ciliary base. We reasoned that the vesicles likely fuse at the base of
151 the primary cilium [60] releasing Gli proteins. Therefore, for continuous trafficking, new vesicles
152 that would carry Gli proteins would need to form. The two potential sources of these vesicles
153 are the Golgi apparatus via the exocytic pathway[61,62] and the plasma membrane by
154 endocytosis[63–65]. Firstly, we inhibited endocytosis using two inhibitors: dynasore[66] and
155 pitstop2[67] in cells expressing constitutively active Gli2. Surprisingly, after 2h of dynasore
156 treatment, we observed an almost complete inhibition of Gli2 ciliary accumulation. This effect

157 was independent of Smo because treatment with two Smo inhibitors cyclopamine and
158 vismodegib did not affect the Gli2(P1-6A) ciliary level (Fig. 5E and Fig. S3A).

159 If the dynasore effects are a consequence of the reduced rate of new vesicle formation, we
160 would expect these effects to be fully reversible once the proper formation of vesicles is
161 restored. We used a pulse-chase assay with 2h vismodegib + dynasore treatment, and then
162 we washed out dynasore from the media and collected cells at several time points. We
163 observed a clear recovery of Gli2 ciliary transport within 1h from the dynasore washout (Fig.
164 5D). This effect was present in both NIH/3T3 cells (Fig. 5D) and in IMCD3 cells (Fig. S3???),
165 suggesting that cells utilizing both the intracellular and extracellular ciliogenesis pathways
166 (NIH/3T3 and IMCD3, respectively[68]) use endocytic vesicles to deliver Gli proteins to cilia.

167 As an alternative to dynasore, we also used another commercial clathrin-dependent
168 endocytosis inhibitor pitstop2. Because of its lethal effect on NIH/3T3 fibroblasts in less than
169 30min, we treated cells with pitstop2 for 15 min, followed by a 30min incubation without the
170 drug. Similar to the dynasore effects, we observed a decrease of Gli2 ciliary level in pitstop2-
171 treated cells (Fig. 5F). Importantly, neither dynasore, nor pitstop2 induced gross
172 morphological changes indicative of toxicity under the conditions used to block endocytosis
173 (Fig. S3B).

174 To determine if the vesicle transport from the cis-Golgi was also important for Gli2 ciliary
175 trafficking, we treated stable HA-Gli2(P1-6A) cells with brefeldin A, a Golgi-disrupting drug[69].
176 We did not observe changes in Gli2 ciliary localization after 2h treatment (Fig. 5G).

177 The stimulation of target gene transcription by Gli2 is enhanced by its localization at the
178 cilium[9,70]. We expected that dynasore would inhibit Hh target gene transcription in cells stably
179 expressing the Gli2(P1-6A). Indeed, the expression of the Hh target gene Gli1 was decreased
180 after dynasore treatment, although the expression of HA-Gli2(P1-6A) was unchanged (Fig. 5H).

181 Rab and Arf proteins mediate Gli2 transport

182 The trafficking of vesicles in cells is guided by the reversible association of small GTPases,
183 especially from the Rab and Arf families[25,71]. Because their association with vesicles and
184 associated proteins is transient, we hypothesized that under the stringent conditions of our
185 initial co-IP/MS, the Gli-associating GTPases may have been washed away from the bait
186 protein. Thus, we performed another co-IP/MS, with less stringent detergents, using HA-
187 Gli2(P1-6A) as bait in cells that either had normal cilia or were devoid of cilia by means of
188 overexpression of a dominant-negative mutant Kif3a motor[72]. We expected the GTPases
189 promoting Gli ciliary trafficking to be associated with Gli2 in ciliated, but not in unciliated cells
190 (Fig. 6A).

191 We identified 200 high-confidence interactors (<10% FDR in the CRAPome database) including
192 the same well-known regulators of Gli, such as SuFu, Kif7, Xpo7, and Spop[53,51,73,74], as well as
193 component proteins of the cilium and basal body (Fig. 6B, Supplementary Table S2). Among
194 proteins associated with Gli2(P1-6A) in ciliated cells were Rab14, Rab5c, Rab11b, Rab18, and
195 Arf4 (Fig. 6C). In addition, we tested two other Rab-family GTPases: the well-known Hh
196 regulator Rab23[75–77] and Rab8, which cooperates with the exocyst in the trafficking of
197 membrane receptors to primary cilium[43,78].

198 Initially, we established by co-IP that Rab14, Rab18, Rab23, and Arf4 proteins interact with
199 Gli2(P1-6A) (Fig. 7A). In contrast, two Rab GTPases that had been implicated in ciliary
200 trafficking of membrane proteins: Rab8 and Rab11a, do not strongly bind to Gli2(P1-6A) (Fig.
201 S4A).

202 Subsequently, we performed loss-of-function experiments using shRNA and CRISPR/Cas9
203 mutagenesis. The knockdown of Rab14, Rab18, and Arf4 caused the reduction of the Gli2(P1-
204 6A) ciliary level (Fig. 7B-D). Likewise, the CRISPR/Cas9-mediated Rab14, Rab18, and Rab23
205 knockout also significantly decreased the Gli2(P1-6A) ciliary accumulation (Fig. 7E). Moreover,
206 we engineered cell lines expressing dominant-negative Rab23S51N and Arf4T31N mutants
207 from doxycycline-inducible promoters. Consistent with shRNA- and CRISPR/Cas9-based
208 experiments, we observed a significant decrease of Gli2(P1-6A) ciliary accumulation in cells
209 expressing Arf4 and Rab23 mutants (Fig.7F).

210 The trafficking of Lkb1, but not Ubxn10, depends on endocytosis and the exocyst

211 We wanted to know if the mechanism of transport to cilia with the use of endocytic vesicles
212 was unique to Gli proteins or more common among other soluble ciliary proteins. For this
213 purpose, we imaged several HA or GFP tagged soluble ciliary candidate proteins: HA-Dvl2[79],
214 Kap3a-EGFP[80], HA-Lkb1[81], HA-Mek1[82], HA-Nbr1[83], HA-Raptor[84], Tbx3-GFP[85], and Ubxn10-
215 GFP[86]. Only two proteins clearly localized at cilia in NIH/3T3: Ubxn10-GFP, and HA-Lkb1 (Fig.
216 8A and Fig. S5).

217 To examine if the ciliary serine-threonine kinase Lkb1 uses an analogous transport mechanism,
218 we treated stable expressing HA-Lkb1 cells with dynasore and observed decreased Lkb1 ciliary
219 level (Fig. 8D). Similar to Gli2, ciliary accumulation of HA-Lkb1 also dropped after the shRNA
220 knockdown of Sec3/5/8 (Fig. 8B). Accordingly, we detected HA-Lkb1 in the endosomal fraction
221 (Fig. 7G). Finally, we observed using co-IP that Lkb1 binds to the exocyst subunits (Fig. 8F).

222 Another soluble ciliary protein that we studied was Ubxn10. Dynasore treatment did not
223 negatively affect the ciliary trafficking of Ubxn10-GFP (Fig. 8E). Unlike for Gli2(P1-6A), we
224 observed no effect of Sec5 knockdown on Ubxn10 ciliary localization (Fig. 8C). Consistent with
225 these results, we detected Ubxn10 predominantly in the cytosolic cell fraction (Fig. 8H).

226

227 ## Discussion

228 The cilium is an essential organelle that relays environmental signals to the nucleus.
229 Nevertheless, the mechanism of the signaling protein delivery to cilia is still poorly
230 understood, especially for soluble proteins. To gain a better understanding of cytoplasmic
231 proteins' transport to cilia we studied Gli transcription factors, large soluble proteins that
232 accumulate at the tip of the cilium before their conversion into transcriptional activators [5,9,11].

233 Using proteomic screening, we found that Gli proteins interact with the exocyst, a complex
234 implicated in ciliary delivery of membrane receptors[23,54]. We found that loss-of-function of
235 the exocyst by RNAi, mitochondrial trap, or drug treatment decreases ciliary localization of
236 the constitutively active mutant Gli2(P1-6A) independently of their effect on transmembrane
237 Hh signaling proteins Ptch and Smo.

238 On a molecular level, we show that the N-terminal region of Gli proteins binds to the
239 subcomplex I of the exocyst, which includes the Sec3/5/6/8 subunits[34,87]. This agrees with our
240 data and published reports suggesting that the N-terminal domain is necessary for the Gli
241 proteins ciliary accumulation[5,9,11]. The N-terminus is, however, not sufficient for Gli ciliary
242 transport, with other domains, particularly the central domain of Gli2/3[5,9] likely participating
243 in other stages of ciliary translocation, such as the passage through the diffusion barrier and
244 the transport to the cilium tip.

245 Our results suggest that soluble cytoplasmic proteins, like Gli2/3, can use the exocyst as a
246 vehicle for intracellular trafficking. The exocyst was shown to collaborate with the BLOC-1
247 complex and IFT20 in the transport of membrane proteins polycystin-2 and fibrocystin to
248 cilia[23]. However, IFT20 does not interact with HA-Gli2(P1-6A) (Fig. S4A). This suggests that the
249 exocyst may mediate Gli protein ciliary trafficking independently of IFT20, which implies that
250 the pathways directing membrane and soluble cilium components are somewhat divergent.
251 Importantly, the exocyst can be transported to the cilium despite IFT20 loss-of-function[23].

252 Interestingly, we found that the exocyst subunits accumulate at the cilium base upon
253 stimulation of the canonical Hh signaling. The most parsimonious explanation of this result is
254 that the exocyst is co-transported with Gli proteins upon pathway activation. Alternatively,
255 the exocyst might be delivered to the cilium base independently of Gli proteins, and then
256 either trap these proteins at the base prior to their translocation to the cilium or promote
257 their accumulation at the cilium indirectly. However, the fact that we see foci of interaction
258 between Gli2 and the exocyst in areas distal to the cilium (Fig. 2B) suggests that the co-
259 transport hypothesis is most likely.

260 Consistent with the requirement of the exocyst in the transport of Gli2 to cilia, it appears that
261 Gli2 is associated, at least transiently, with intracellular vesicles. Interestingly, the subunits of
262 the exocyst that most strongly interact with Gli2 are positioned away from the putative lipid-
263 facing surface of the complex[34,87], indicating that the exocyst may form a tether between
264 vesicle lipids and soluble proteins. Structural ciliary proteins had been previously found to be
265 attached to the outer surfaces of intracellular vesicles carrying ciliary membrane proteins in
266 *Chlamydomonas*[88]. We now provide functional data that corroborate and extend these
267 findings. Protein delivery by vesicles to the cilium is persistent and essential for maintaining

268 proper cilium function and structure[89,90]. Thus, the strategy of using vesicles as universal
269 carriers of proteins, both soluble and membrane-embedded, to cilia, solves the logistical
270 problem of homing many protein classes onto the tiny cilium base.

271 The trafficking of vesicles in cells is coordinated by the small GTPases from the Rab and Arf
272 families. Intriguingly, we found that Rab14, Rab18, Rab23, and Arf4, interact with Gli2 and are
273 essential for its accumulation in the ciliary compartment. The Rab14 GTPase localizes at early
274 endosomes and plays a role in protein exchange between the endosomes and the Golgi
275 compartment[91–94], and exocytic vesicle targeting[95]. On the other hand, Rab18 is usually
276 associated with the endoplasmic reticulum and lipid droplets[96,97]. Intriguingly, we identify
277 COPI and TRAPP complex components in Gli2(P1-6A) and Gli3 interactomes, and these
278 complexes have been implicated in lipid droplet recruitment of Rab18[98]. This suggests that Gli
279 may recruit Rab18 via TRAPPII and COPI to promote ciliary trafficking. Interestingly, all three
280 of the above GTPases: Rab18, Rab14, and Arf4, were recently identified as proximity
281 interactors of the cilium base-localized kinase Ttbk2[99], strengthening the case for their
282 involvement in the targeting of Gli-laden vesicles to the cilium.

283 Finally, Rab23 had previously been implicated in Hh signaling and ciliary transport of
284 receptors[100]. Rab23 is described as a negative regulator of the Hh pathway but several
285 different mechanisms have been proposed, from affecting Smo to directly regulating Gli
286 proteins[76,101,75]. Here, we propose Rab23 as one of the key players in the trafficking of Gli
287 transcription factors into the primary cilium. This is consistent with the recently discovered
288 role of Rab23 in the transport of another soluble protein, Kif17, to primary cilia and with the
289 ciliary and early endosome enrichment of Rab23[102,103].

290 In addition to Rab family GTPases, we found Gli2 to associate with Arf4, which functions in
291 sorting ciliary cargo at the Golgi and is a crucial regulator of ciliary receptor trafficking[104,105].
292 Arf4 binds the ciliary targeting signal of rhodopsin and controls the assembly of the Rab11a-
293 Rabin8-Rab8 module for the proper delivery of cargo to the ciliary base[106]. Although Rab8 and
294 Rab11a were found to cooperate with both the exocyst and Arf4[106] in the targeting of ciliary
295 cargos, we found that the expression of dominant-negative Rab8 and Rab11a did not
296 negatively affect Gli2 ciliary accumulation, with Rab8 DN actually promoting higher Gli2
297 accumulation in cilia (Fig. S4B). Moreover, we did not find Rab8 or Rab11a among interactors
298 of Gli2 and Gli3 in our co-IP/MS datasets. Instead, among Gli2 interactors was a Rab11a
299 ortholog Rab11b, which had also been implicated in ciliogenesis and found to associate with
300 Rab8[107,108]. Disentangling the roles of the two Rab11 orthologs as well as Rab8/Rabin8 in the
301 trafficking of soluble ciliary components will be an interesting subject for future studies.

302 The data from loss of function studies of small GTPases did not allow us to identify a known
303 source of vesicles that participated in Gli2 trafficking to cilia. Many of the implicated Rab/Arf
304 proteins had been known to associate both with Golgi-derived exocytic vesicles and with
305 plasma membrane-derived endosomes. To decipher the relative importance of these two
306 potential vesicle sources, we used pharmacological inhibitors to show that Gli2 is likely
307 delivered to cilia via endocytic vesicle trafficking rather than the canonical secretory pathway.

308 In addition to Gli2, other soluble ciliary proteins can adopt a similar transport mechanism.
309 Specifically, we show that Lkb1 levels at primary cilia drop upon exocyst loss-of-function and
310 inhibition of endocytosis. Like Gli2, Lkb1 associates with intracellular vesicles and interacts
311 with the exocyst. Intriguingly, Lkb1 has been shown to be able to associate directly with
312 plasma membrane phospholipids in addition to its nuclear and ciliary localization[109]. It will be
313 interesting to determine if direct phospholipid binding is important for the targeting of Lkb1
314 to vesicles and its ciliary transport and whether phospholipid and exocyst association are
315 synergistic. Incidentally, the exocyst and Lkb1 show similar specific affinity for phosphatidic
316 acid[109,110]. It is tempting to speculate that other proteins that rely on vesicles for ciliary
317 delivery, such as Gli2, may also show some affinity for membrane lipids even in the absence
318 of exocyst tethering.

319 In contrast to Gli2 and Lkb1, another soluble ciliary component Ubxn10 localizes at the cilium
320 normally in cells depleted of Sec5 or treated with dynasore. This suggests that while the
321 vesicle-mediated transport is important for the ciliary localization of some cytoplasmic
322 proteins, others use different routes of ciliary trafficking. Ubxn10 binds directly to the IFT-B
323 complex via IFT38/CLUAP1 [86], so it may be delivered to the primary cilium with the IFT
324 particles. Alternatively, the dynamics of Ubxn10 exchange at the cilium may be slower than
325 that of Gli2 or Lkb1, which prevents us from observing changes in its localization upon
326 dynasore treatment. Nevertheless, the lack of effect of Sec5 knockdown on Ubxn10 ciliary
327 accumulation argues against such an interpretation.

328 In summary, we describe a novel mechanism for the transport of soluble cytoplasmic proteins
329 to primary cilia, which relies on the association of these proteins with dynamically cycling
330 endocytic vesicles. While we identify several key players in the ciliary trafficking of these
331 vesicles, further work will dissect the precise sequence of events that are involved in this
332 process. In particular, it will be interesting to discover potential similarities and differences
333 between the canonical ciliary targeting pathways for membrane proteins, such as polycystin
334 2, fibrocystin, Smo, and rhodopsin with those described here for soluble ciliary proteins. Our
335 work brings us closer to gaining a broad understanding of ciliary trafficking and the
336 coordinated transport of proteins among membrane compartments.

337 Acknowledgments

338 We would like to thank Marta Miączyńska, Małgorzata Maksymowicz, Jarosław Cendrowski,
339 and the members of the CeNT Bio PI discussion group, and the Laboratory of Molecular and
340 Cellular Signalling for insightful discussion and helpful suggestions. We thank M. Raman, A.
341 Moon, D. Mick, and P. Avasthi for sharing their reagents with us and Addgene contributors for
342 making their plasmids available (see Table 1). This work was supported by the following grants
343 from the National Science Centre (NCN): SONATA BIS 2014/14/E/NZ3/00033 and PRELUDIUM
344 2018/29/N/NZ3/01523.

345

346 # Materials and methods

347 ## Constructs and molecular cloning

348 Gli2/3 constructs were cloned based on the Gli2(P1-6A) mutant previously described[55] tagged
349 with the N-terminal 3xHA. Initially, Gli2 fragments were amplified by PCR and then cloned into
350 the pENTR2B (Life Technologies) vector by Gibson assembly[111] using the NEBuilder® HiFi DNA
351 Assembly Master Mix (NEB). Subsequently, the constructs were shuttled into pEF/FRT/V5-
352 DEST (Life Technologies) using the Gateway method (Gateway LR Clonase II mix; Life
353 Technologies). Plasmids with Sec3/5/8, Rab8/11/14/18, and Arf4 on the pEGFP vector were
354 ordered from the Addgene site (Tab. 1). Rab23 wild type and mutant cDNA sequences were
355 obtained by DNA synthesis (DNA Strings; Thermo) and cloned by Gibson assembly into the
356 LT3GEPIR plasmid ordered from addgene (Tab. 1). Tom20 sequence was amplified from mouse
357 cDNA and then fused with mScarlet cloned from pmScaret (addgene, Tab. 1) and Sec5 by
358 Gibson assembly in the pEGFP-C3 vector with the EGFP sequence removed by restriction
359 digestion. Other soluble proteins sequences of Dvl2, Nbr1, Mek1, Lkb1, Raptor were amplified
360 from mouse cDNA and cloned into the pENTR2B with 3xHA tag vector by Gibson assembly.
361 Ubnx10 was cloned from pHAGE-NGFP-UBXD3 - gift from M. Raman[86]. Tbx3 was cloned from
362 the construct with Tbx3-Myc - a gift from A. Moon[85]. pEGFP-Kap3a was a gift from P. Avasthi
363 and pEGFP-Rab11a was a gift from M. Miaczynska.

364 Tab. 1. Plasmids used in our experiments ordered from the addgene site

	Plasmid name	Addgene No.	Gift from	References
1	pEGFP-C3-Sec3	#53755	Channing Der	112
2	pEGFP-C3-Sec5	#53756	Channing Der	112
3	pEGFP-C3-Sec8	#53758	Channing Der	112
4	pmScarlet_C1	#85042	Dorus Gadella	113
5	pLKO.1 - TRC cloning vector	#10878	David Root	114
6	pLKO.1 - blast	#25566	Keith Mostov	115
7	lentiCas9-Blast	#52962	Feng Zhang	116
8	LT3GEPIR	#111177	Johannes Zuber	117
9	lentiGuide-Puro	#52963	Feng Zhang	116
10	pRSV-Rev	#12253	Didier Trono	118
11	pMDLg/pRRE	#12251	Didier Trono	118
12	pMD2.G	#12259	Didier Trono	unpublished
13	EGFP-Rab14	#49549	Marci Scidmore	119
14	EGFP-Rab18	#49550	Marci Scidmore	119
15	Arf4-GFP	#39556	Paul Melancon	120
16	pCAG/hArf4(T31N)-HA	#79405	Kazuhisa Nakayama	121
17	GFP-rab11 DN	#12678	Richard Pagano	122
18	pGFP-Rab8A	#24898	Maxence Nachury	123
19	pGFP-Rab8A[T22N]	#24899	Maxence Nachury	123
20	pLenti-IFT20-EGFP	#118032	Ken Ichi Takemaru	unpublished

365 ## Cell culture

366 HEK293T (ATCC) and NIH/3T3 Flp-In (Thermo) cells were maintained in media composed of
367 DMEM (high glucose; Biowest), sodium pyruvate (Thermo), stable glutamine (Biowest), non-
368 essential amino acids (Thermo), 10% fetal bovine serum (EurX), and penicillin/streptomycin
369 solution (Thermo). mIMCD3 Flp-In cells (gift from D. Mick[124]) were cultured in DMEM/F-12
370 (Gibco) media supplemented with 2mM stable glutamine (Biowest), 10% fetal bovine serum
371 (EurX), and penicillin/streptomycin solution (Thermo). HA-Gli2(P1-6A) and HA-LKB1 NIH/3T3
372 and mIMCD3 stable cell lines were generated using the Flp-In system according to the
373 manufacturer's protocols (Thermo Fisher). Stable cell lines were reselected with hygromycin
374 on every other passage to preserve selection pressure.

375 To stimulate ciliogenesis the cells were cultured in the same medium but containing 0.5% FBS
376 for 24h before fixing. For activation of the Hh pathway, we used SAG (Smoothened agonist)
377 treatment 200nM for 24h. Transient transfections of cells we performed using the JetPrime
378 reagent (Polyplus) according to the manufacturer's protocol.

379 All inhibitors were suspended in DMSO and used with indicated times. The following
380 concentrations of inhibitors were used: dynasore (40µM, Sigma), endosidin2 (200µM, Sigma),
381 pitstop2 (30µM, Sigma), brefeldin A (5µg/ml, Sigma).

382 ## Large scale co-IP/MS on Gli3

383 NIH/3T3 cells were cultured to confluence on 50 15cm dishes and starved overnight to
384 promote ciliogenesis. They were treated with 100nM SAG for 4h. The cells were fractionated
385 into "nuclear" and "cytoplasmic" fractions as previously described[125]. Briefly, cells were
386 washed 2x with ice-cold PBS and 2x with ice-cold 10mM HEPES pH 7.4. They were left on ice
387 in 10mM HEPES for 10 min. to swell. The HEPES buffer was removed and the cells were scraped
388 in ice-cold SEAT (sucrose, EDTA, acetic acid, triethanolamine) buffer with protease and
389 phosphatase inhibitors and homogenized using a Dounce homogenizer with nuclei release and
390 integrity monitored microscopically. "Nuclear" and "cytoplasmic" fractions were separated
391 using two rounds of centrifugation at 900xg for 5 min. at 4°C. The supernatant from the first
392 centrifugation was collected as the "cytoplasmic" fraction, and the pellet from the first
393 centrifugation was resuspended in SEAT buffer and centrifuged again. The pellet from the
394 second centrifugation was collected as the "nuclear" fraction. The "cytoplasmic" fraction was
395 supplemented with Tris (to a concentration of 50mM), NaCl (to a concentration of 150mM),
396 Nonidet P-40 (to a concentration of 2%), sodium deoxycholate (to a concentration of 0.25%),
397 DTT (to a concentration of 1mM), and protease inhibitors and incubated for 45 min. at 4°C.
398 Afterwards, the "cytoplasmic" lysate was centrifuged at 20,000xg for 45 min, and the
399 supernatant was used for immunoprecipitation. The "nuclear" pellet was lysed for 45 min in
400 a buffer containing 50mM Tris, 150mM NaCl, 2% Nonidet P-40, 0.25 sodium deoxycholate,
401 1mM DTT, and protease and phosphatase inhibitors. The "nuclear" lysate was cleared by
402 centrifugation at 20,000xg for 30 min. at 4°C and used for immunoprecipitation. Each fraction
403 was immunoprecipitated overnight with 150µL Dynabeads-Protein G (Invitrogen) covalently
404 cross-linked with goat-anti-Gli3 (AF3690; R&D Systems; 30µg antibody per fraction). The
405 beads were washed with the following buffers: harsh RIPA lysis buffer (50mM Tris pH 7.4,
406 150mM NaCl, 2% Nonidet P-40, 500mM LiCl, 1mM DTT, 0.25% sodium deoxycholate, 0.1%

407 SDS, protease and phosphatase inhibitors), RIPA lysis buffer supplemented with 0.8M urea,
408 and mild 0.1% NP-40 lysis buffer (50mM Tris pH 7.4, 150mM NaCl, 0.1% Nonidet P-40, 1mM
409 DTT, 1% glycerol, phosphatase inhibitors). The samples were eluted from beads using
410 preheated 2x Laemmli sample buffer without DTT at 85°C for 5 min. The samples were then
411 reduced and alkylated using DTT and iodoacetamide and loaded onto a 6% SDS-PAGE gel. The
412 gel was stained using the GelCode Blue reagent (Pierce) and prominent bands were excised
413 using a sterile scalpel and submitted for further processing to MS Bioworks (Ann Arbor, MI).
414 The bands were destained and subjected to in-gel digest using trypsin. Each gel digest was
415 analyzed by nano LC/MS/MS with a Waters NanoAcquity HPLC system interfaced to a
416 ThermoFisher LTQ Orbitrap Velos. Peptides were loaded on a trapping column and eluted over
417 a 75µm analytical column at 350nL/min; both columns were packed with Jupiter Proteo resin
418 (Phenomenex). The mass spectrometer was operated in data-dependent mode, with MS
419 performed in the Orbitrap at 60,000 FWHM resolution and MS/MS performed in the LTQ. The
420 fifteen most abundant ions were selected for MS/MS. Data were searched using a local copy
421 of Mascot with the following parameters: Enzyme: Trypsin, Database: IPI Mouse v3.75
422 (forward and reverse appended with common contaminants), Fixed modification:
423 Carbamidomethyl (C), Variable modifications: Oxidation (M), Acetyl (N-term, K), Pyro-Glu (N-
424 term Q), Deamidation (N,Q), Phospho (S,T,Y), GlyGly (K), Mass values: Monoisotopic, Peptide
425 Mass Tolerance: 10 ppm, Fragment Mass Tolerance: 0.5 Da, Max Missed Cleavages: 2. Mascot
426 DAT files were parsed into the Scaffold algorithm for validation, filtering, and to create a
427 nonredundant list per sample. Data were filtered using a minimum protein value of 90%, a
428 minimum peptide value of 50% (Prophet scores), and requiring at least two unique peptides
429 per protein.

430 To determine high-confidence Gli3 interactors, we rejected all proteins found in more than
431 10% of negative control affinity purification/MS experiments in the CRAPome database[126]
432 (FDR < 10%). Enrichment of proteins representing specific Gene Ontology terms was
433 performed using PANTHER with GO-Slim Cellular Component and GO-Slim Biological Process
434 terms [127].

435 Large scale co-IP/MS on HA-Gli2 (P1-6A) in ciliated and non-ciliated cells

436 NIH/3T3 cells stably expressing HA-Gli2 (P1-6A) were transduced either with the control vector
437 or with a retroviral vector encoding the dominant-negative variant of Kif3a (headless – amino
438 acids 441-701 of the mouse Kif3a; dnKif3a) and selected with puromycin to eliminate
439 untransduced cells. Each cell line was expanded from a single clone and ciliogenesis or lack
440 thereof was verified by immunofluorescence.

441 Both cell lines were starved for 36h and lysed in a gentle lysis buffer (50mM Tris pH 7.4,
442 150mM NaCl, 0.1% Nonidet P-40, 5% glycerol, protease and phosphatase inhibitors) and
443 scraped at 4°C. The lysate was clarified for 30min at 15,000xg and the supernatant was
444 immunoprecipitated for 2h at 4°C with Dynabeads-protein G covalently coupled to the rat
445 anti-HA antibody (Roche). The beads were washed 3x5 min. with the lysis buffer and 1x5min
446 with the lysis buffer with the addition of 350mM NaCl (total NaCl concentration 500mM).
447 Protein was eluted from beads using 2x Laemmli sample buffer at 37°C for 30min with
448 vigorous mixing (500rpm).

449 Eluted proteins were submitted for mass spectrometric protein identification to MS Bioworks
450 (Ann Arbor, MI). The entire amount of sample was separated ~1.5cm on a 10% Bis-Tris Novex
451 mini-gel (Invitrogen) using the MES buffer system. The gels were stained with coomassie and
452 excised into ten equally sized segments. Gel segments were processed using a robot (ProGest,
453 DigiLab) with the following protocol: Washed with 25mM ammonium bicarbonate followed
454 by acetonitrile. Reduced with 10mM dithiothreitol at 60°C followed by alkylation with 50mM
455 iodoacetamide at RT. Digested with trypsin (Promega) at 37°C for 4h. Quenched with formic
456 acid and the supernatant was analyzed directly without further processing.

457 The gel digests were analyzed by nano LC/MS/MS with a Waters M-class HPLC system
458 interfaced to a ThermoFisher Fusion Lumos. Peptides were loaded on a trapping column and
459 eluted over a 75µm analytical column at 350nL/min; both columns were packed with Luna C18
460 resin (Phenomenex). A 30min gradient was employed (5h LC/MS/MS per sample). The mass
461 spectrometer was operated in data-dependent mode, with MS and MS/MS performed in the
462 Orbitrap at 60,000 FWHM resolution and 15,000 FWHM resolution, respectively. APD was
463 turned on. The instrument was run with a 3s cycle for MS and MS/MS. Data were searched
464 using a local copy of Mascot with the following parameters: Enzyme: Trypsin, Database:
465 Swissprot Mouse (concatenated forward and reverse plus common contaminants), Fixed
466 modification: Carbamidomethyl (C), Variable modifications: Oxidation (M), Acetyl (Protein N-
467 term), Deamidation (NQ), Mass values: Monoisotopic, Peptide Mass Tolerance: 10 ppm,
468 Fragment Mass Tolerance: 0.02 Da, Max Missed Cleavages: 2. Mascot DAT files were parsed
469 into the Scaffold software for validation, filtering, and to create a nonredundant list per
470 sample. Data were filtered at 1% protein and peptide level FDR and requiring at least two
471 unique peptides per protein.

472 ## Viral transduction

473 For lentivirus production, we transfected HEK293T cells with pRSV-rev, pMDLg/pRRE, pMD2.G
474 lentiviral packaging vectors (addgene, Tab. 1) and the construct encoding our protein or
475 shRNA or sgRNA of interest, and then after 2 days, we collected the virus-containing medium
476 and added it to target cells. We used puromycin to select transduced cells.

477 ## siRNA mediated knockdown

478 For siRNA-mediated knockdown of Sec5, we used the Sec5 ON-TARGET plus siRNA set of four
479 siRNAs with non-targeting controls (Horizon Dharmacon). For siRNA transfection, we used
480 Lipofectamine RNAiMAX (Thermofisher). Each siRNA was introduced at 40 pmol/well on a 24-
481 well plate for 48h.

482 ## shRNA mediated knockdown

483 shRNAs were cloned into pLKO.1-TRC cloning vector (Tab. 1). Targeting sequences were
484 designed using the BlockIT software from the Thermo-Fisher website.

485 ## CRISPR-Cas9-mediated mutagenesis

486 CRISPR-Cas9-mediated mutagenesis was performed on NIH/3T3 Flp-In cells stably expressing
487 HA-Gli2(P1-6A) and Cas9 (Tab. 1). sgRNA sequences were designed using the Broad Institute
488 sgRNA designer tool [128] and cloned into the pLentiGuide-puro vector (addgene, Tab. 1). We

489 transduced the target cells with lentiviruses carrying the sgRNA of interest and either fixed
490 72h later or subjected to antibiotic selection.

491 Tab. 2. Sequences used for shRNA knockdown, CRISPR edition, and qPCR primers.

name	sequence
shRNA-Sec3	GGAGGTGGACCAGATTGAACT
shRNA-Sec5	GCATACGGCCGAAGAGATAAA
shRNA-Sec8	GCAGGAGCTAAAGCAGATTGT
shRNA-Rab14	CGGTTACACGGAGCTACTATA
shRNA-Rab18	TATCATGGCAGTGAGTATTTG
shRNA-Arf4	CGGTTACACGGAGCTACTATA
shRNA-Luciferase	GCTGGAGAGCAACTGCATAAG
sgRNA Rab23	AAAGACTACAAGAAAACCAT
sgRNA Rab14	CATATAACCACTTAAGCAGC
sgRNA Rab18	ATACTCATCATCGGCGAGAG
sgRNA Arf4	GATCGTGAAAGAATCCAGGA
qPCR Rab14 F	GGTTCAGAGCGGTTACACG
qPCR Rab14 R	TGAGATTCCTTGCGTCTGTC
qPCR Rab18 F	GCACGCAAGCATTCTATGTTG
qPCR Rab18 R	AGCTTGACTCCTTTGTTCTGG
qPCR Arf4 F	AGGATCTGCCAAACGCTATG
qPCR Arf4 R	CCTCATACAGACCAGTTCCTTG
qPCR Sec3 F	TCGCGCTGAGAAAAGATGAC
qPCR Sec3 R	TTCTTGCCAGCTTTGCAGAC
qPCR Sec5 F	CGGAGGTGCAAGTTTTCA AG
qPCR Sec5 R	GCATGGAGGTCGGAAAGA TAC
qPCR Sec8 F	AATTGACCACAGCCATTCGC
qPCR Sec8 R	TCATCCCGTTTGCAATGCAG

492

493 ## Immunostaining and microscopy.

494 Cells were cultured on glass coverslips. After low-serum starvation to promote ciliogenesis,
495 we fixed cells in 4% [*w/v*] paraformaldehyde in PBS for 15min at room temperature (RT) and
496 then washed 3 x 10min in phosphate buffer saline (PBS). Subsequently, cells were blocked and
497 permeabilized in 5% [*w/v*] donkey serum in 0.2% [*w/v*] Triton X-100 in PBS. We incubated cells
498 with the primary antibodies diluted in blocking buffer overnight at 4°C. Next, we washed the
499 coverslips 3 x 10min with 0.05% [*w/v*] Triton X-100 in PBS, followed by incubation with
500 secondary antibodies in the blocking buffer for 1 hour at RT. Cells were washed as above and
501 mounted onto slides using a fluorescent mounting medium with DAPI (ProLong Diamond,
502 Thermo). We acquired images on an inverted Olympus IX-73 fluorescent microscope equipped
503 with a 63x uPLANAPO oil objective and the Photometrics Evolve 512 Delta camera. For

504 superresolution microscopy, we used the Zeiss LSM800 confocal microscope with the Airyscan
505 detector and Plan Apochromat 63x/1.4 Oil DIC objective.

506 For the quantitative analysis of fluorescence intensities, images were acquired with the same
507 settings of exposure time, gain, offset, and illumination. Fluorescent intensities were
508 measured in a semi-supervised manner by a custom ImageJ script. To calculate the Gli ciliary
509 accumulation, we calculated the $\log_{10}$ values of the ratios of intensities of the fluorescent
510 signal at the tip of the primary cilium and the surrounding background in each cell.

511 Tab. 3. Antibodies used for western blot, immunofluorescence staining, and proximity ligation
512 assay

Antibody	Application	Company	Ref No.
Primary antibodies	Western blot (WB), Immunofluorescence (IF)		
anti-HA High Affinity	WB (1:1000); IF (1:2000)	Roche	11867423001
anti-HA	WB (1:1000)	BioLegend	901501
anti-GFP	WB (1:1000)	Genetex	GTX113617
anti-Arl13b	IF (1:2000)	Proteintech	17711-1-AP
anti-Sec5	WB (1:500); IF (1:200); PLA	Proteintech	12751-1-AP
anti-Sec5	WB (1:2000)	Proteintech	66011-1-Ig
anti-Sec3	WB (1:1000); IF (1:500)	Proteintech	11690-1-AP
anti-Sec8	WB (1:300)	Proteintech	11913-1-AP
anti-α-tubulin	WB (1:1000)	Sigma	T6199
anti-beta-actin	WB (1:1000)	Sigma	A1978-100UL
anti-Gli2	WB (1:1000)	home-made by Davids biotechnologie	
anti-Gli2	PLA	R&D Systems	AF3635
anti-Gli3	WB (1:1000)	R&D Systems	AF3690
anti-Pericentrin	IF (1:200)	BD Biosciences	611814
anti-EEA1	WB (1:1000)	BD Biosciences	610456
anti-acetylated tubulin	IF (1:1000)	Sigma	T6793
Secondary antibodies			
anti-mouse alexa-488	IF (1:1000)	Jackson Immunoresearch	715-545-151
anti-rabbit alexa-488	IF (1:1000)	Jackson Immunoresearch	711-545-152
anti-rat alexa-488	IF (1:1000)	Jackson Immunoresearch	712-545-153
anti-rabbit alexa-Cy3	IF (1:1000)	Jackson Immunoresearch	711-165-152
anti-mouse alexa-594	IF (1:1000)	Jackson Immunoresearch	715-585-151
anti-rabbit alexa-594	IF (1:1000)	Jackson Immunoresearch	711-585-152
anti-rat alexa-647	IF (1:1000)	Jackson Immunoresearch	712-605-153
HRP anti-mouse	WB (1:2500)	BioLegend	405306
HRP anti-rabbit	WB (1:2500)	BioLegend	406401
HRP anti-goat	WB (1:2500)	Sigma	A5420

513

514 ## Co-immunoprecipitation

515 We performed co-immunoprecipitation using Pierce Anti-HA Magnetic Beads (Life
516 Technologies) or using Dynabeads-protein G (Thermo) magnetic beads with primary
517 antibodies (anti-GFP Genetex No#GTX113717; anti-Sec5 Proteintech No#12751-1-AP) cross-
518 linked using dimethyl pimelimidate (Life Technologies).

519 For the production of whole-cell lysates, cells were lysed in 4°C in lysis buffer (50 mM Tris at
520 pH 7.4, 1% NP-40 [*v*/*v*], 150 mM NaCl, 0.25% sodium deoxycholate [*v*/*v*], protease inhibitor
521 cocktail [1× EDTA-free protease inhibitors, Sigma], 10mM NaF). 1/10 part of the clarified lysate
522 was saved as an input fraction, and the rest was subjected to immunoprecipitation.

523 After adding beads, binding of the protein of interest was performed overnight with gentle
524 rotation at 4°C. The next day, beads were washed 4 x 10min in 4°C in the same lysis buffer to
525 remove unbound proteins, and complexes were eluted off the beads using 2x SDS sample
526 buffer at 37C for 30min. We analyzed the composition of eluent using the SDS-PAGE and
527 Western Blot method.

528 ## SDS-PAGE and Western Blot

529 Proteins were denaturated for 30min at 65°C and resolved by SDS-PAGE. Afterward, we
530 performed electrotransfer onto a nitrocellulose membrane. Immunocomplexes were
531 detected using an enhanced chemiluminescence detection system (Clarity or Clarity Max, Bio-
532 rad) on Amersham Imager 680 and 800 as 16-bit grayscale TIFF files. The molecular weight of
533 proteins was estimated with pre-stained protein markers (Bio-rad).

534 ## Proximity Ligation Assay

535 We performed the proximity ligation assay[129] using the Duolink PLA Kit (Merck) according to
536 the manufacturer's protocol. Anti-Sec5 and anti-Gli2 primary antibodies (Tab. 3) were used to
537 detect sites of interaction between the proteins in NIH/3T3 Flp-In cells**.**

538 ## Endosome Isolation

539 The Trident Endosome Isolation Kit (Genetex) was used to fractionate cell lysates according to
540 the manufacturer's protocol.

541 ## Electron Microscopy

542 HEK293 cells expressing EGFP-Gli2(P-16A) were fixed on the dish with 4% PFA in 0.2M
543 phosphate buffer and 0.25% sucrose. The samples were sent to Biocenter Oulu Electron
544 Microscopy Core Facility and there processed for EM and immunogold labeled with anti-GFP.
545 Imaging was performed on Sigma HD VP FE-SEM equipped with ET-SE and In-lens SE detectors,
546 VPSE G3 detector for low vacuum mode, and 5Q-BSD detector.

547 ## Data analysis

548 The statistical data analysis was performed using Microsoft Excel and R/RStudio. For the
549 processing of the fluorescence images, we used the FiJi/ImageJ suite. Statistical significance
550 was calculated using Student's t-test for experiments involving two experimental groups, or
551 ANOVA and Tukey posthoc test for multiple comparisons.

552 ## References

553 1. Briscoe, J. & Thérond, P. P. The mechanisms of Hedgehog signalling and its roles in
554 development and disease. *Nat. Rev. Mol. Cell Biol.* **14**, 416–429 (2013).
555 2. Niewiadomski, P. *et al.* Gli Proteins: Regulation in Development and Cancer. *Cells* **8**,
556 (2019).
557 3. Huangfu, D. *et al.* Hedgehog signalling in the mouse requires intraflagellar transport
558 proteins. *Nature* **426**, 83–87 (2003).
559 4. Goetz, S. C. & Anderson, K. V. The primary cilium: a signalling centre during vertebrate
560 development. *Nat. Rev. Genet.* **11**, 331–344 (2010).
561 5. Zeng, H., Jia, J. & Liu, A. Coordinated translocation of mammalian Gli proteins and
562 suppressor of fused to the primary cilium. *PloS One* **5**, e15900 (2010).
563 6. Tukachinsky, H., Lopez, L. V. & Salic, A. A mechanism for vertebrate Hedgehog signaling:
564 recruitment to cilia and dissociation of SuFu–Gli protein complexes. *J. Cell Biol.* **191**,
565 415–428 (2010).
566 7. Niewiadomski, P., Zhujiang, A., Youssef, M. & Waschek, J. A. Interaction of PACAP with
567 Sonic hedgehog reveals complex regulation of the hedgehog pathway by PKA. *Cell.*
568 *Signal.* **25**, 2222–2230 (2013).
569 8. Barzi, M., Berenguer, J., Menendez, A., Alvarez-Rodriguez, R. & Pons, S. Sonic-
570 hedgehog-mediated proliferation requires the localization of PKA to the cilium base. *J.*
571 *Cell Sci.* **123**, 62–69 (2010).
572 9. Santos, N. & Reiter, J. F. A central region of Gli2 regulates its localization to the primary
573 cilium and transcriptional activity. *J. Cell Sci.* **127**, 1500–1510 (2014).
574 10. Haycraft, C. J. *et al.* Gli2 and Gli3 Localize to Cilia and Require the Intraflagellar
575 Transport Protein Polaris for Processing and Function. *PLOS Genet.* **1**, e53 (2005).
576 11. Han, Y. *et al.* Regulation of Gli ciliary localization and Hedgehog signaling by the PY-
577 NLS/karyopherin-β2 nuclear import system. *PLOS Biol.* **15**, e2002063 (2017).
578 12. Lin, Y.-C. *et al.* Chemically inducible diffusion trap at cilia reveals molecular sieve–like
579 barrier. *Nat. Chem. Biol.* **9**, 437–443 (2013).
580 13. Nachury, M. V., Seeley, E. S. & Jin, H. Trafficking to the ciliary membrane: how to get
581 across the periciliary diffusion barrier? *Annu. Rev. Cell Dev. Biol.* **26**, 59–87 (2010).
582 14. Ocbina, P. J. R., Eggenschwiler, J. T., Moskowitz, I. & Anderson, K. V. Complex
583 interactions between genes controlling trafficking in primary cilia. *Nat. Genet.* **43**, 547–
584 553 (2011).
585 15. Tran, P. V. *et al.* THM1 negatively modulates mouse sonic hedgehog signal transduction
586 and affects retrograde intraflagellar transport in cilia. *Nat. Genet.* **40**, 403–410 (2008).
587 16. Qin, J., Lin, Y., Norman, R. X., Ko, H. W. & Eggenschwiler, J. T. Intraflagellar transport
588 protein 122 antagonizes Sonic Hedgehog signaling and controls ciliary localization of
589 pathway components. *Proc. Natl. Acad. Sci. U. S. A.* **108**, 1456–1461 (2011).
590 17. Torrado, B., Graña, M., Badano, J. L. & Irigoín, F. Ciliary Entry of the Hedgehog
591 Transcriptional Activator Gli2 Is Mediated by the Nuclear Import Machinery but Differs
592 from Nuclear Transport in Being Imp-α/β1-Independent. *PLOS ONE* **11**, e0162033
593 (2016).
594 18. Barnfield, P. C., Zhang, X., Thanabalasingham, V., Yoshida, M. & Hui, C. Negative
595 regulation of Gli1 and Gli2 activator function by Suppressor of fused through multiple
596 mechanisms. *Differentiation* **73**, 397–405 (2005).

597 19. Breslow, D. K., Koslover, E. F., Seydel, F., Spakowitz, A. J. & Nachury, M. V. An in vitro
598 assay for entry into cilia reveals unique properties of the soluble diffusion barrier. *J. Cell*
599 *Biol.* **203**, 129–147 (2013).
600 20. Kee, H. L. *et al.* A size-exclusion permeability barrier and nucleoporins characterize a
601 ciliary pore complex that regulates transport into cilia. *Nat. Cell Biol.* **14**, 431–437
602 (2012).
603 21. Cassioli, C. & Baldari, C. T. A Ciliary View of the Immunological Synapse. *Cells* **8**, (2019).
604 22. Milenkovic, L., Scott, M. P. & Rohatgi, R. Lateral transport of Smoothened from the
605 plasma membrane to the membrane of the cilium. *J. Cell Biol.* **187**, 365–374 (2009).
606 23. Monis, W. J., Faundez, V. & Pazour, G. J. BLOC-1 is required for selective membrane
607 protein trafficking from endosomes to primary cilia. *J. Cell Biol.* **216**, 2131–2150 (2017).
608 24. Lu, L. & Madugula, V. Mechanisms of ciliary targeting: entering importins and Rabs.
609 *Cell. Mol. Life Sci. CMLS* **75**, 597–606 (2018).
610 25. Nassari, S., Del Olmo, T. & Jean, S. Rabs in Signaling and Embryonic Development. *Int. J.*
611 *Mol. Sci.* **21**, (2020).
612 26. Bigge, B. M., Rosenthal, N. E. & Avasthi, P. *Initial ciliary assembly in Chlamydomonas*
613 *requires Arp2/3 complex-dependent endocytosis*. 2020.11.24.396002
614 https://www.biorxiv.org/content/10.1101/2020.11.24.396002v3 (2021)
615 doi:10.1101/2020.11.24.396002.
616 27. Takai, Y., Sasaki, T. & Matozaki, T. Small GTP-Binding Proteins. *Physiol. Rev.* **81**, 153–208
617 (2001).
618 28. Yoshimura, S.-I., Egerer, J., Fuchs, E., Haas, A. K. & Barr, F. A. Functional dissection of
619 Rab GTPases involved in primary cilium formation. *J. Cell Biol.* **178**, 363–369 (2007).
620 29. Kawamura, N. *et al.* Delivery of endosomes to lysosomes via microautophagy in the
621 visceral endoderm of mouse embryos. *Nat. Commun.* **3**, 1–10 (2012).
622 30. Singh, S. K., Gui, M., Koh, F., Yip, M. C. & Brown, A. Structure and activation mechanism
623 of the BBSome membrane protein trafficking complex. *eLife* **9**, e53322.
624 31. Wingfield, J. L., Lechtreck, K.-F. & Lorentzen, E. Trafficking of ciliary membrane proteins
625 by the intraflagellar transport/BBSome machinery. *Essays Biochem.* **62**, 753–763
626 (2018).
627 32. Lobo, G. P. *et al.* The exocyst is required for photoreceptor ciliogenesis and retinal
628 development. *J. Biol. Chem.* **292**, 14814–14826 (2017).
629 33. Martin-Urdiroz, M., Deeks, M. J., Horton, C. G., Dawe, H. R. & Jourdain, I. The Exocyst
630 Complex in Health and Disease. *Front. Cell Dev. Biol.* **4**, 24 (2016).
631 34. Mei, K. *et al.* Cryo-EM structure of the exocyst complex. *Nat. Struct. Mol. Biol.* **25**, 139–
632 146 (2018).
633 35. Xiong, X. *et al.* An association between type Iγ PI4P 5-kinase and Exo70 directs E-
634 cadherin clustering and epithelial polarization. *Mol. Biol. Cell* **23**, 87–98 (2012).
635 36. Jose, M. *et al.* A quantitative imaging-based screen reveals the exocyst as a network
636 hub connecting endocytosis and exocytosis. *Mol. Biol. Cell* **26**, 2519–2534 (2015).
637 37. He, B., Xi, F., Zhang, X., Zhang, J. & Guo, W. Exo70 interacts with phospholipids and
638 mediates the targeting of the exocyst to the plasma membrane. *EMBO J.* **26**, 4053–
639 4065 (2007).
640 38. Zhang, X. *et al.* Membrane association and functional regulation of Sec3 by
641 phospholipids and Cdc42. *J. Cell Biol.* **180**, 145–158 (2008).
642 39. Lalli, G. RalA and the exocyst complex influence neuronal polarity through PAR-3 and
643 aPKC. *J. Cell Sci.* **122**, 1499–1506 (2009).

644 40. Das, A. *et al.* RalA promotes a direct exocyst-Par6 interaction to regulate polarity in
645 neuronal development. *J. Cell Sci.* **127**, 686–699 (2014).
646 41. Zhang, X. *et al.* Cdc42 interacts with the exocyst and regulates polarized secretion. *J.*
647 *Biol. Chem.* **276**, 46745–46750 (2001).
648 42. Seixas, C. *et al.* Arl13b and the exocyst interact synergistically in ciliogenesis. *Mol. Biol.*
649 *Cell* **27**, 308–320 (2016).
650 43. Feng, S. *et al.* A Rab8 guanine nucleotide exchange factor-effector interaction network
651 regulates primary ciliogenesis. *J. Biol. Chem.* **287**, 15602–15609 (2012).
652 44. Fogelgren, B. *et al.* The exocyst protein Sec10 interacts with Polycystin-2 and
653 knockdown causes PKD-phenotypes. *PLoS Genet.* **7**, e1001361 (2011).
654 45. Zuo, X., Guo, W. & Lipschutz, J. H. The exocyst protein Sec10 is necessary for primary
655 ciliogenesis and cystogenesis in vitro. *Mol. Biol. Cell* **20**, 2522–2529 (2009).
656 46. Zuo, X. *et al.* The exocyst acting through the primary cilium is necessary for renal
657 ciliogenesis, cystogenesis, and tubulogenesis. *J. Biol. Chem.* **294**, 6710–6718 (2019).
658 47. Polgar, N., Lee, A. J., Lui, V. H., Napoli, J. A. & Fogelgren, B. The exocyst gene Sec10
659 regulates renal epithelial monolayer homeostasis and apoptotic sensitivity. *Am. J.*
660 *Physiol. Cell Physiol.* **309**, C190-201 (2015).
661 48. Chen, J. K., Taipale, J., Young, K. E., Maiti, T. & Beachy, P. A. Small molecule modulation
662 of Smoothened activity. *Proc. Natl. Acad. Sci.* **99**, 14071–14076 (2002).
663 49. Mellacheruvu, D. *et al.* The CRAPome: a contaminant repository for affinity purification-
664 mass spectrometry data. *Nat. Methods* **10**, 730–736 (2013).
665 50. Breslow, D. K. *et al.* A CRISPR-based screen for Hedgehog signaling provides insights
666 into ciliary function and ciliopathies. *Nat. Genet.* **50**, 460–471 (2018).
667 51. Han, Y., Shi, Q. & Jiang, J. Multisite interaction with Sufu regulates Ci/Gli activity
668 through distinct mechanisms in Hh signal transduction. *Proc. Natl. Acad. Sci. U. S. A.*
669 **112**, 6383–6388 (2015).
670 52. Markiewicz, Ł., Uśpieński, T., Baran, B., Niedziółka, S. M. & Niewiadomski, P. Xpo7
671 negatively regulates Hedgehog signaling by exporting Gli2 from the nucleus. *Cell.*
672 *Signal.* **80**, 109907 (2021).
673 53. Maurya, A. K. *et al.* Positive and negative regulation of Gli activity by Kif7 in the
674 zebrafish embryo. *PLoS Genet.* **9**, e1003955 (2013).
675 54. Ahmed, S. M. *et al.* Exocyst dynamics during vesicle tethering and fusion. *Nat. Commun.*
676 **9**, 1–17 (2018).
677 55. Niewiadomski, P. *et al.* Gli protein activity is controlled by multisite phosphorylation in
678 vertebrate Hedgehog signaling. *Cell Rep.* **6**, 168–181 (2014).
679 56. Huang, P. *et al.* Structural Basis of Smoothened Activation in Hedgehog Signaling. *Cell*
680 **175**, 295–297 (2018).
681 57. Rohatgi, R., Milenkovic, L. & Scott, M. P. Patched1 regulates hedgehog signaling at the
682 primary cilium. *Science* **317**, 372–376 (2007).
683 58. Luo, G., Zhang, J. & Guo, W. The role of Sec3p in secretory vesicle targeting and exocyst
684 complex assembly. *Mol. Biol. Cell* **25**, 3813–3822 (2014).
685 59. Zhang, C. *et al.* Endosidin2 targets conserved exocyst complex subunit EXO70 to inhibit
686 exocytosis. *Proc. Natl. Acad. Sci. U. S. A.* **113**, E41-50 (2016).
687 60. Ghossoub, R. *et al.* Morphological and Functional Characterization of the Ciliary Pocket
688 by Electron and Fluorescence Microscopy. *Methods Mol. Biol. Clifton NJ* **1454**, 35–51
689 (2016).

690 61. Sung, C.-H. & Leroux, M. R. The roles of evolutionarily conserved functional modules in
691 cilia-related trafficking. *Nat. Cell Biol.* **15**, 1387–1397 (2013).
692 62. Lee, S.-H. *et al.* Export of membrane proteins from the Golgi complex to the primary
693 cilium requires the kinesin motor, KIFC1. *FASEB J. Off. Publ. Fed. Am. Soc. Exp. Biol.* **32**,
694 957–968 (2018).
695 63. Leroux, M. R. Taking vesicular transport to the cilium. *Cell* **129**, 1041–1043 (2007).
696 64. Goldenring, J. R. Recycling endosomes. *Curr. Opin. Cell Biol.* **35**, 117–122 (2015).
697 65. Naslavsky, N. & Caplan, S. Endocytic membrane trafficking in the control of centrosome
698 function. *Curr. Opin. Cell Biol.* **65**, 150–155 (2020).
699 66. Macia, E. *et al.* Dynasore, a cell-permeable inhibitor of dynamin. *Dev. Cell* **10**, 839–850
700 (2006).
701 67. Dutta, D., Williamson, C. D., Cole, N. B. & Donaldson, J. G. Pitstop 2 is a potent inhibitor
702 of clathrin-independent endocytosis. *PloS One* **7**, e45799 (2012).
703 68. Stuck, M. W., Chong, W. M., Liao, J.-C. & Pazour, G. J. Rab34 is necessary for early
704 stages of intracellular ciliogenesis. *Curr. Biol.* **31**, 2887-2894.e4 (2021).
705 69. Miller, S. G., Carnell, L. & Moore, H. H. Post-Golgi membrane traffic: brefeldin A inhibits
706 export from distal Golgi compartments to the cell surface but not recycling. *J. Cell Biol.*
707 **118**, 267–283 (1992).
708 70. Kim, J., Kato, M. & Beachy, P. A. Gli2 trafficking links Hedgehog-dependent activation of
709 Smoothened in the primary cilium to transcriptional activation in the nucleus. *Proc.*
710 *Natl. Acad. Sci.* **106**, 21666–21671 (2009).
711 71. Stenmark, H. Rab GTPases as coordinators of vesicle traffic. *Nat. Rev. Mol. Cell Biol.* **10**,
712 513–525 (2009).
713 72. Lin, F. *et al.* Kidney-specific inactivation of the KIF3A subunit of kinesin-II inhibits renal
714 ciliogenesis and produces polycystic kidney disease. *Proc. Natl. Acad. Sci. U. S. A.* **100**,
715 5286–5291 (2003).
716 73. Markiewicz, Ł., Uśpieński, T., Niedziółka, S. M. & Niewiadomski, P. Xpo7 negatively
717 regulates Hedgehog signaling by exporting Gli2 from the nucleus. *bioRxiv*
718 2020.01.31.928408 (2020) doi:10.1101/2020.01.31.928408.
719 74. Umberger, P. A. & Ogden, S. K. SPOP and CUL3 Modulate the Sonic Hedgehog Signal
720 Response Through Controlled Degradation of GLI Family Transcription Factors. *Front.*
721 *Cell Dev. Biol.* **9**, 710295 (2021).
722 75. Eggenschwiler, J. T., Bulgakov, O. V., Qin, J., Li, T. & Anderson, K. V. Mouse Rab23
723 regulates hedgehog signaling from smoothened to Gli proteins. *Dev. Biol.* **290**, 1–12
724 (2006).
725 76. Hor, C., Lo, J., Cham, A., Leong, W. Y. & Goh, E. Multifaceted functions of Rab23 on
726 primary cilium- and Hedgehog signaling-mediated cerebellar granule cell proliferation.
727 *J. Neurosci. Off. J. Soc. Neurosci.* JN-RM-3005-20 (2021) doi:10.1523/JNEUROSCI.3005-
728 20.2021.
729 77. Wang, Y., Ng, E. L. & Tang, B. L. Rab23: what exactly does it traffic? *Traffic Cph. Den.* **7**,
730 746–750 (2006).
731 78. Das, A. & Guo, W. Rabs and the exocyst in ciliogenesis, tubulogenesis and beyond.
732 *Trends Cell Biol.* **21**, 383–386 (2011).
733 79. Lee, K. H. *et al.* Identification of a novel Wnt5a-CK1ε-Dvl2-Plk1-mediated primary cilia
734 disassembly pathway. *EMBO J.* **31**, 3104–3117 (2012).
735 80. Morris, R. L. *et al.* Redistribution of the kinesin-II subunit KAP from cilia to nuclei during
736 the mitotic and ciliogenic cycles in sea urchin embryos. *Dev. Biol.* **274**, 56–69 (2004).

737 81. Viau, A. *et al.* Cilia-localized LKB1 regulates chemokine signaling, macrophage
738 recruitment, and tissue homeostasis in the kidney. *EMBO J.* **37**, (2018).
739 82. Clement, D. L. *et al.* PDGFRα signaling in the primary cilium regulates NHE1-dependent
740 fibroblast migration via coordinated differential activity of MEK1/2-ERK1/2-p90RSK and
741 AKT signaling pathways. *J. Cell Sci.* **126**, 953–965 (2013).
742 83. Peixoto, E. *et al.* HDAC6-dependent ciliophagy is involved in ciliary loss and
743 cholangiocarcinoma growth in human cells and murine models. *Am. J. Physiol.*
744 *Gastrointest. Liver Physiol.* **318**, G1022–G1033 (2020).
745 84. Lai, Y. & Jiang, Y. Reciprocal Regulation between Primary Cilia and mTORC1. *Genes* **11**,
746 E711 (2020).
747 85. Emechebe, U. *et al.* T-box3 is a ciliary protein and regulates stability of the Gli3
748 transcription factor to control digit number. *eLife* **5**, e07897 (2016).
749 86. Raman, M. *et al.* Systematic VCP-UBXD Adaptor Network Proteomics Identifies a Role
750 for UBXN10 in Regulating Ciliogenesis. *Nat. Cell Biol.* **17**, 1356–1369 (2015).
751 87. Picco, A. *et al.* The In Vivo Architecture of the Exocyst Provides Structural Basis for
752 Exocytosis. *Cell* **168**, 400-412.e18 (2017).
753 88. Wood, C. R. & Rosenbaum, J. L. Proteins of the ciliary axoneme are found on
754 cytoplasmic membrane vesicles during growth of cilia. *Curr. Biol. CB* **24**, 1114–1120
755 (2014).
756 89. Nachury, M. V. & Mick, D. U. Establishing and regulating the composition of cilia for
757 signal transduction. *Nat. Rev. Mol. Cell Biol.* **20**, 389–405 (2019).
758 90. Pedersen, L. B., Veland, I. R., Schrøder, J. M. & Christensen, S. T. Assembly of primary
759 cilia. *Dev. Dyn. Off. Publ. Am. Assoc. Anat.* **237**, 1993–2006 (2008).
760 91. Reed, S. E. *et al.* A role for Rab14 in the endocytic trafficking of GLUT4 in 3T3-L1
761 adipocytes. *J. Cell Sci.* **126**, 1931–1941 (2013).
762 92. Proikas-Cezanne, T., Gaugel, A., Frickey, T. & Nordheim, A. Rab14 is part of the early
763 endosomal clathrin-coated TGN microdomain. *FEBS Lett.* **580**, 5241–5246 (2006).
764 93. Junutula, J. R. *et al.* Rab14 Is Involved in Membrane Trafficking between the Golgi
765 Complex and Endosomes. *Mol. Biol. Cell* **15**, 2218–2229 (2004).
766 94. Ueno, H., Huang, X., Tanaka, Y. & Hirokawa, N. KIF16B/Rab14 Molecular Motor
767 Complex Is Critical for Early Embryonic Development by Transporting FGF Receptor.
768 *Dev. Cell* **20**, 60–71 (2011).
769 95. Lu, R. & Wilson, J. M. Rab14 specifies the apical membrane through Arf6-mediated
770 regulation of lipid domains and Cdc42. *Sci. Rep.* **6**, (2016).
771 96. Dejgaard, S. Y. *et al.* Rab18 and Rab43 have key roles in ER-Golgi trafficking. *J. Cell Sci.*
772 **121**, 2768–2781 (2008).
773 97. Martin, S. & Parton, R. G. Characterization of Rab18, a lipid droplet-associated small
774 GTPase. *Methods Enzymol.* **438**, 109–129 (2008).
775 98. Li, C. *et al.* COPI-TRAPPII activates Rab18 and regulates its lipid droplet association.
776 *EMBO J.* **36**, 441–457 (2017).
777 99. Loukil, A., Barrington, C. & Goetz, S. C. A complex of distal appendage–associated
778 kinases linked to human disease regulates ciliary trafficking and stability. *Proc. Natl.*
779 *Acad. Sci.* **118**, (2021).
780 100. Leaf, A. & Von Zastrow, M. Dopamine receptors reveal an essential role of IFT-B, KIF17,
781 and Rab23 in delivering specific receptors to primary cilia. *eLife* **4**, e06996 (2015).
782 101. Boehlke, C. *et al.* Differential role of Rab proteins in ciliary trafficking: Rab23 regulates
783 smoothened levels. *J. Cell Sci.* **123**, 1460–1467 (2010).

784 102. Lim, Y. S. & Tang, B. L. A role for Rab23 in the trafficking of Kif17 to the primary cilium.
785 *J. Cell Sci.* **128**, 2996–3008 (2015).
786 103. Evans, T. M., Ferguson, C., Wainwright, B. J., Parton, R. G. & Wicking, C. Rab23, a
787 negative regulator of hedgehog signaling, localizes to the plasma membrane and the
788 endocytic pathway. *Traffic Cph. Den.* **4**, 869–884 (2003).
789 104. Follit, J. A. *et al.* Arf4 is required for Mammalian development but dispensable for
790 ciliary assembly. *PLoS Genet.* **10**, e1004170 (2014).
791 105. Gillingham, A. K. & Munro, S. The small G proteins of the Arf family and their regulators.
792 *Annu. Rev. Cell Dev. Biol.* **23**, 579–611 (2007).
793 106. Deretic, D., Lorentzen, E. & Fresquez, T. The ins and outs of the Arf4-based ciliary
794 membrane-targeting complex. *Small GTPases* 1–12 (2019)
795 doi:10.1080/21541248.2019.1616355.
796 107. Oguchi, M. E., Okuyama, K., Homma, Y. & Fukuda, M. A comprehensive analysis of Rab
797 GTPases reveals a role for Rab34 in serum starvation-induced primary ciliogenesis. *J.*
798 *Biol. Chem.* **295**, 12674–12685 (2020).
799 108. Westlake, C. J. *et al.* Primary cilia membrane assembly is initiated by Rab11 and
800 transport protein particle II (TRAPPII) complex-dependent trafficking of Rabin8 to the
801 centrosome. *Proc. Natl. Acad. Sci.* **108**, 2759–2764 (2011).
802 109. Dogliotti, G. *et al.* Membrane-binding and activation of LKB1 by phosphatidic acid is
803 essential for development and tumour suppression. *Nat. Commun.* **8**, 15747 (2017).
804 110. Synek, L. *et al.* Plasma membrane phospholipid signature recruits the plant exocyst
805 complex via the EXO70A1 subunit. *Proc. Natl. Acad. Sci.* **118**, (2021).
806 111. Grozdanov, P. N. & MacDonald, C. C. Generation of plasmid vectors expressing FLAG-
807 tagged proteins under the regulation of human elongation factor-1α promoter using
808 Gibson assembly. *J. Vis. Exp. JoVE* (2015) doi:10.3791/52235.
809 112. Martin, T. D. *et al.* Ral and Rheb GTPase activating proteins integrate mTOR and GTPase
810 signaling in aging, autophagy, and tumor cell invasion. *Mol. Cell* **53**, 209–220 (2014).
811 113. Bindels, D. S. *et al.* mScarlet: a bright monomeric red fluorescent protein for cellular
812 imaging. *Nat. Methods* **14**, 53–56 (2017).
813 114. Moffat, J. *et al.* A lentiviral RNAi library for human and mouse genes applied to an
814 arrayed viral high-content screen. *Cell* **124**, 1283–1298 (2006).
815 115. Bryant, D. M. *et al.* A molecular network for de novo generation of the apical surface
816 and lumen. *Nat. Cell Biol.* **12**, 1035–1045 (2010).
817 116. Sanjana, N. E., Shalem, O. & Zhang, F. Improved vectors and genome-wide libraries for
818 CRISPR screening. *Nat. Methods* **11**, 783–784 (2014).
819 117. Fellmann, C. *et al.* An optimized microRNA backbone for effective single-copy RNAi. *Cell*
820 *Rep.* **5**, 1704–1713 (2013).
821 118. Dull, T. *et al.* A third-generation lentivirus vector with a conditional packaging system. *J.*
822 *Virol.* **72**, 8463–8471 (1998).
823 119. Huang, B. *et al.* The Anaplasma phagocytophilum-occupied vacuole selectively recruits
824 Rab-GTPases that are predominantly associated with recycling endosomes. *Cell.*
825 *Microbiol.* **12**, 1292–1307 (2010).
826 120. Chun, J., Shapovalova, Z., Dejgaard, S. Y., Presley, J. F. & Melançon, P. Characterization
827 of class I and II ADP-ribosylation factors (Arfs) in live cells: GDP-bound class II Arfs
828 associate with the ER-Golgi intermediate compartment independently of GBF1. *Mol.*
829 *Biol. Cell* **19**, 3488–3500 (2008).

121. Nakai, W. *et al.* ARF1 and ARF4 regulate recycling endosomal morphology and retrograde transport from endosomes to the Golgi apparatus. *Mol. Biol. Cell* **24**, 2570–2581 (2013).
122. Choudhury, A. *et al.* Rab proteins mediate Golgi transport of caveola-internalized glycosphingolipids and correct lipid trafficking in Niemann-Pick C cells. *J. Clin. Invest.* **109**, 1541–1550 (2002).
123. Nachury, M. V. *et al.* A core complex of BBS proteins cooperates with the GTPase Rab8 to promote ciliary membrane biogenesis. *Cell* **129**, 1201–1213 (2007).
124. Mick, D. U. *et al.* Proteomics of Primary Cilia by Proximity Labeling. *Dev. Cell* **35**, 497–512 (2015).
125. Humke, E. W., Dorn, K. V., Milenkovic, L., Scott, M. P. & Rohatgi, R. The output of Hedgehog signaling is controlled by the dynamic association between Suppressor of Fused and the Gli proteins. *Genes Dev.* **24**, 670–682 (2010).
126. Mellacheruvu, D. *et al.* The CRAPome: a contaminant repository for affinity purification-mass spectrometry data. *Nat. Methods* **10**, 730–736 (2013).
127. Mi, H. *et al.* PANTHER version 16: a revised family classification, tree-based classification tool, enhancer regions and extensive API. *Nucleic Acids Res.* **49**, D394–D403 (2021).
128. Doench, J. G. *et al.* Optimized sgRNA design to maximize activity and minimize off-target effects of CRISPR-Cas9. *Nat. Biotechnol.* **34**, 184–191 (2016).
129. Söderberg, O. *et al.* Direct observation of individual endogenous protein complexes in situ by proximity ligation. *Nat. Methods* **3**, 995–1000 (2006).

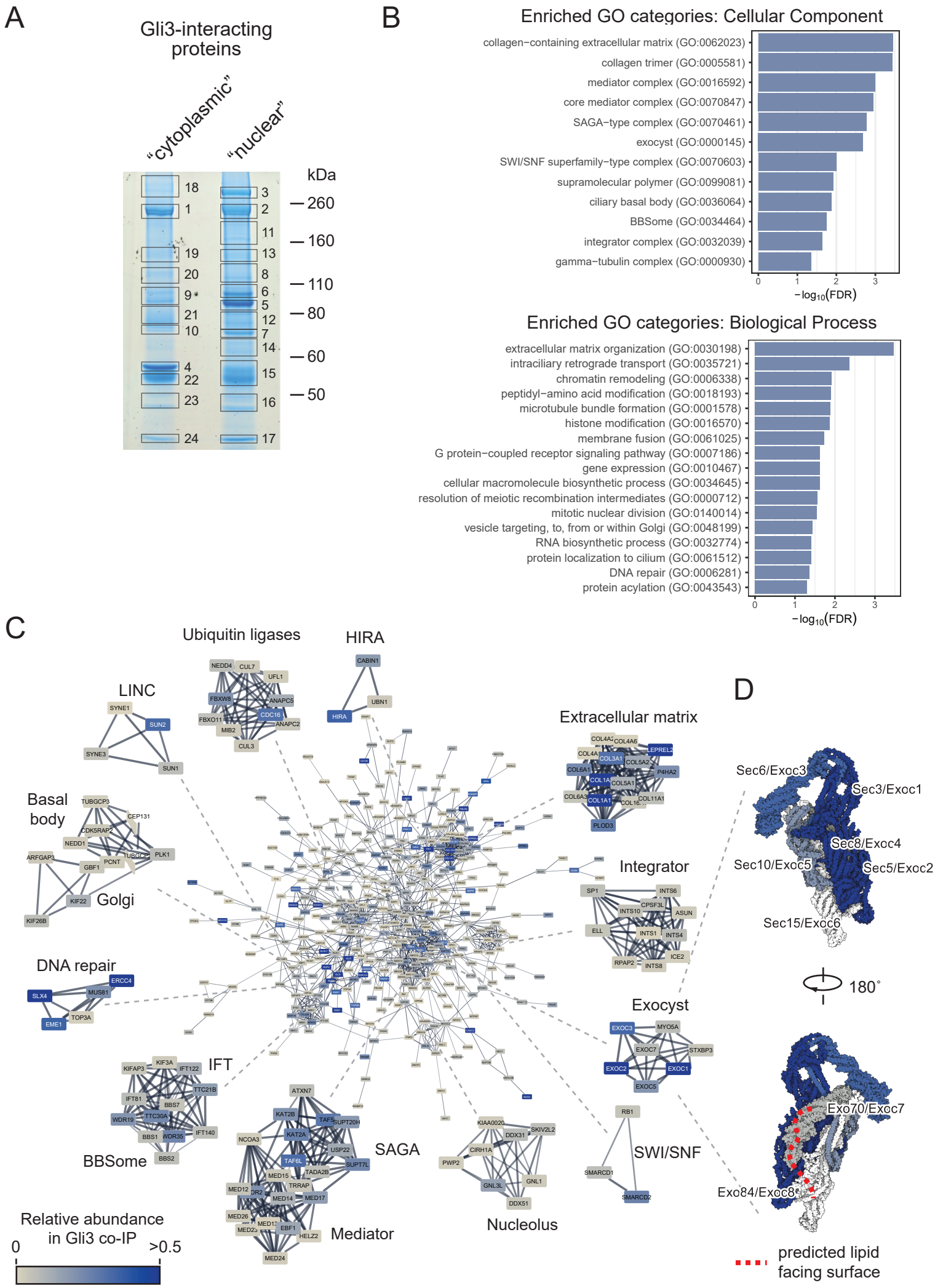
A
Gli3-interacting proteins
"cytoplasmic"
"nuclear"
kDa
260
160
110
80
60
50
B
Enriched GO categories: Cellular Component
collagen−containing extracellular matrix (GO:0062023)
collagen trimer (GO:0005581)
mediator complex (GO:0016592)
core mediator complex (GO:0070847)
SAGA−type complex (GO:0070461)
exocyst (GO:0000145)
SWI/SNF superfamily−type complex (GO:0070603)
supramolecular polymer (GO:0099081)
ciliary basal body (GO:0036064)
BBSome (GO:0034464)
integrator complex (GO:0032039)
gamma−tubulin complex (GO:0000930)
−log10(FDR)
Enriched GO categories: Biological Process
extracellular matrix organization (GO:0030198)
intraciliary retrograde transport (GO:0035721)
chromatin remodeling (GO:0006338)
peptidyl−amino acid modification (GO:0018193)
microtubule bundle formation (GO:0001578)
histone modification (GO:0016570)
membrane fusion (GO:0061025)
G protein−coupled receptor signaling pathway (GO:0007186)
gene expression (GO:0010467)
cellular macromolecule biosynthetic process (GO:0034645)
resolution of meiotic recombination intermediates (GO:0000712)
mitotic nuclear division (GO:0140014)
vesicle targeting, to, from or within Golgi (GO:0048199)
RNA biosynthetic process (GO:0032774)
protein localization to cilium (GO:0061512)
DNA repair (GO:0006281)
protein acylation (GO:0043543)
−log10(FDR)
C
Ubiquitin ligases
HIRA
LINC
Extracellular matrix
Basal body
Golgi
Integrator
DNA repair
Exocyst
IFT
BBSome
SAGA
SWI/SNF
Nucleolus
Mediator
Relative abundance in Gli3 co-IP
0
>0.5
D
Sec6/Exoc3
Sec3/Exoc1
Sec8/Exoc4
Sec10/Exoc5
Sec5/Exoc2
Sec15/Exoc6
180˚
Exo70/Exoc7
Exo84/Exoc8
predicted lipid facing surface

Fig. 1 Gli3 interactome is enriched for proteins involved in ciliary transport of vesicles

(A) NIH/3T3 Flp-In cells were treated with 100nM SAG for 4h, roughly fractionated into a “cytoplasmic” and “nuclear” fraction, and each fraction was pulled down using magnetic beads coated with the anti-Gli3 antibody. Proteins were resolved on SDS-PAGE, the gel was stained with coomassie brilliant blue and prominent bands were excised for mass spectrometry-based protein ID. Shown is the image of the coomassie-stained gel with each of the excised bands indicated and numbered. Gli3 is enriched in bands 1 (“cytoplasmic”) and 2 (“nuclear”). (B) MS-identified proteins from all bands were pooled and common MS-AP contaminants (>10% FDR from the CRAPome database 30) were removed. PANTHER 103 was used to find overrepresented Gene Ontology (GO) terms in the “PANTHER GO – Slim Biological Process” and “PANTHER GO – Slim Cellular Component” categories. Top-level enriched GO terms are shown with their corresponding -log10(FDR) values. (C) High confidence Gli3 interactors identified by MS were connected into a network using the STRING 106 plugin in Cytoscape. Shown is the main protein network with the node color representing the approximate relative abundance of the protein in the Gli3 interactome and the edge thickness corresponding to the confidence of connection between proteins in the STRING database. Also shown are highly interconnected sub-networks identified using MCODE clustering, which typically corresponds to protein complexes or multiprotein functional units. (D) The exocyst complex structure (PDB ID: 5yfp ref 26) was rendered using Illustrate 107 with each subunit colored according to its abundance in Gli3 IP/MS as in C. Subunits not identified in our experiment are rendered in white. The red dashed line corresponds to the predicted surface of the exocyst complex that comes into contact with the plasma membrane lipids 26. Each subunit is labeled with its alternative gene names.

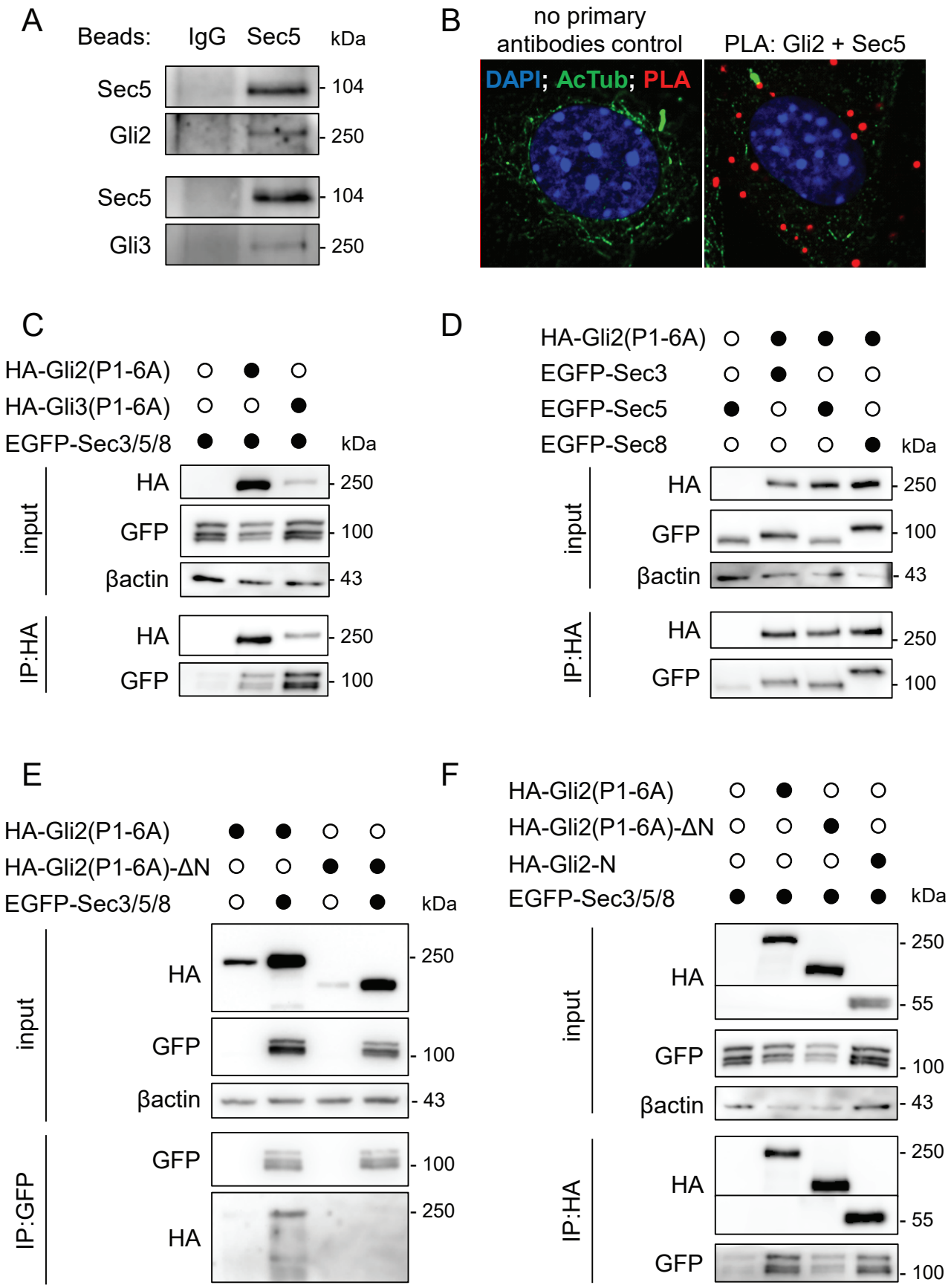

Fig. 2 Exocyst subunits interact with Gli2 and Gli3

(A) Co-immunoprecipitation of endogenous Sec5 with Gli2 and Gli3. Beads were coated with anti-Sec5 antibodies. Rabbit IgG was used as a control. (B) Proximity Ligation Assay with anti-Gli2 and anti-Sec5 antibodies in NIH/3T3 mouse fibroblasts. Sites of interaction are marked in red. Cilia were stained with anti-acetylated tubulin (green), and nuclei with DAPI (blue) (C) Co-immunoprecipitation of overexpressed HA-Gli2(P1-6A) and HA-Gli3(P1-6A) with the exocyst subunits Sec3, Sec5, and Sec8 tagged with EGFP in HEK293T cells using anti-HA beads (D) Co-immunoprecipitation of overexpressed HA-Gli2(P1-6A) with single exocyst subunits Sec3, Sec5 and Sec8 tagged with EGFP in HEK293T cells using anti-HA beads (E) Reciprocal co-immunoprecipitation of overexpressed EGFP-tagged Sec3, Sec5 and Sec8 with HA-Gli2(P1-6A) constructs using anti-GFP beads. (F) Co-immunoprecipitation of overexpressed HA-Gli2(P1-6A) truncation constructs with the exocyst subunits Sec3, Sec5, and Sec8 tagged with EGFP in HEK293T cells using anti-HA beads.

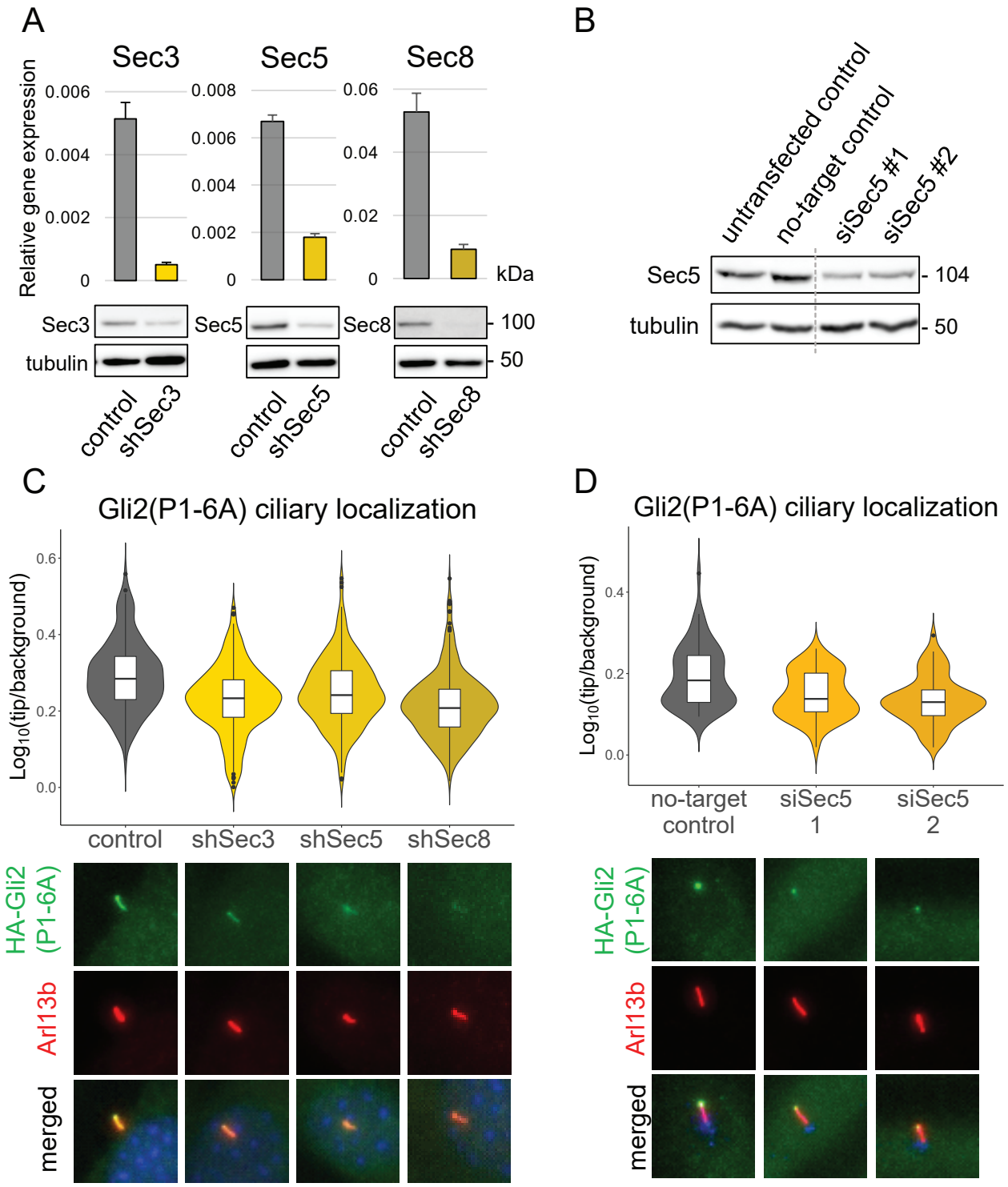

Fig. 3 Knockdown of exocyst subunits decreases Gli2 ciliary localization

(A) mRNA expression levels of the indicated genes in cells stable expressing Gli2(P1-6A) and transduced with shRNA against each of the genes were measured using qRT-PCR. Control cells were transduced with shRNA against luciferase. The protein level of the indicated proteins was detected by western blot. (B) The protein level of Sec5 in cells transfected with siRNA against Sec5 or non-targeting control siRNA. (C) Relative localization at the cilium tip of stably expressed Gli2(P1-6A) in cells with shRNA knockdown of Sec3, Sec5, and Sec8. Results are presented as violin plots of log-transformed ratios of fluorescence intensity of anti-HA staining at cilia tips to the intensity in the surrounding background. Cilia per variant n > 170. Student's t-test analysis control-shSec3 p-value = 5.399e-12; control-shSec5 p-value = 2.206e-06; control-shSec8 p-value < 2.2e-16. Representative images of Gli2(P1-6A) ciliary localization for each condition are presented below. Arl13b was used as a ciliary marker. (D) Relative localization at the cilium tip of Gli2(P1-6A) in cells transfected with indicated siRNAs. Fluorescence intensities were quantified as in Fig. 3C from n > 60 cilia per group. Student's t-test for no-target control-siRNA2 p-value = 0.0001015; for no-target control-siRNA3 p-value = 1.581e-06. Representative images of Gli2(P1-6A) ciliary localization for each condition are presented below. Arl13b was used as a ciliary marker and pericentrin (blue) as a basal body marker.

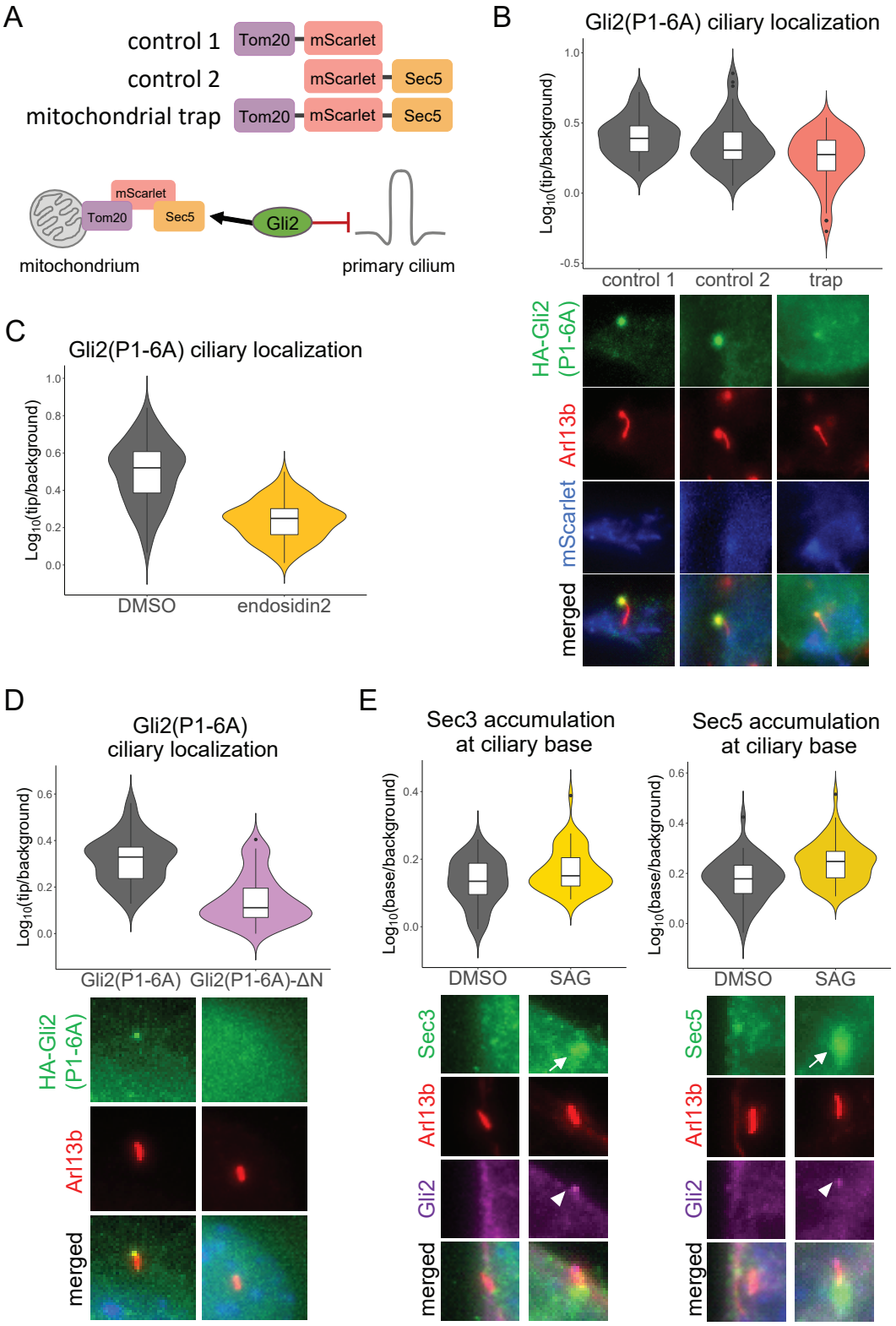

Fig. 4 Impairment of exocyst function reduces Gli2 ciliary localization

(A) Schematic representation of the exocyst mitochondrial trap constructs (top) and assay (bottom) (B) Relative localization at the cilium tip of Gli2(P1-6A) in HEK293T cells co-transfected with the HA-Gli2(P1-6A) and the indicated constructs in n > 40 cilia. Fluorescence intensities were quantified as in Fig. 3C. Student's test for control 1 vs trap p-value = 4.28e-06; control 2 vs. trap p-value = 0.002. Representative images of Gli2(P1-6A) ciliary localization are presented below. (C) The exocyst inhibitor endosidin2 blocks the ciliary accumulation of Gli2(P1-6A). Relative localization at the cilium tip of Gli2(P1-6A) in NIH/3T3 cells expressing HA-Gli2(P1-6A) treated for 2h with DMSO or 200μM endosidin2 was measured in n > 100 cilia per group. Fluorescence intensities were quantified as in Fig. 3C. Student's t-test p-value < 2.2e-16 (D) Gli2(P1-6A)-ΔN is largely excluded from the tip of cilia. Relative localization at the cilium tip of Gli2 constructs stably expressed in NIH/3T3 cells. Fluorescence intensities were quantified as in Fig. 3C in n > 50 cilia per group. Student's t-test p-value = 2.2e-14. Representative images are presented below. Arl13b was used as a ciliary marker. (E) Effect of Smoothened agonist (SAG) treatment (24h; 200nM) on the accumulation of Sec3 and Sec5 at the ciliary base in NIH/3T3 cells. Cells were stained with anti-Sec3 or anti-Sec5 and the ciliary marker acetylated α-tubulin (AcTub). Relative localization at the cilium base was measured in n > 40 cells per group as in Fig. 3C. Student's t-test Sec3: control vs SAG p-value = 0.005; Sec5: control vs SAG p-value = 4.6e-05. Representative images for each condition are presented below. Arl13b was used as a ciliary marker. White arrows show Sec3/5 accumulation and white arrowheads show Gli2 ciliary accumulation.

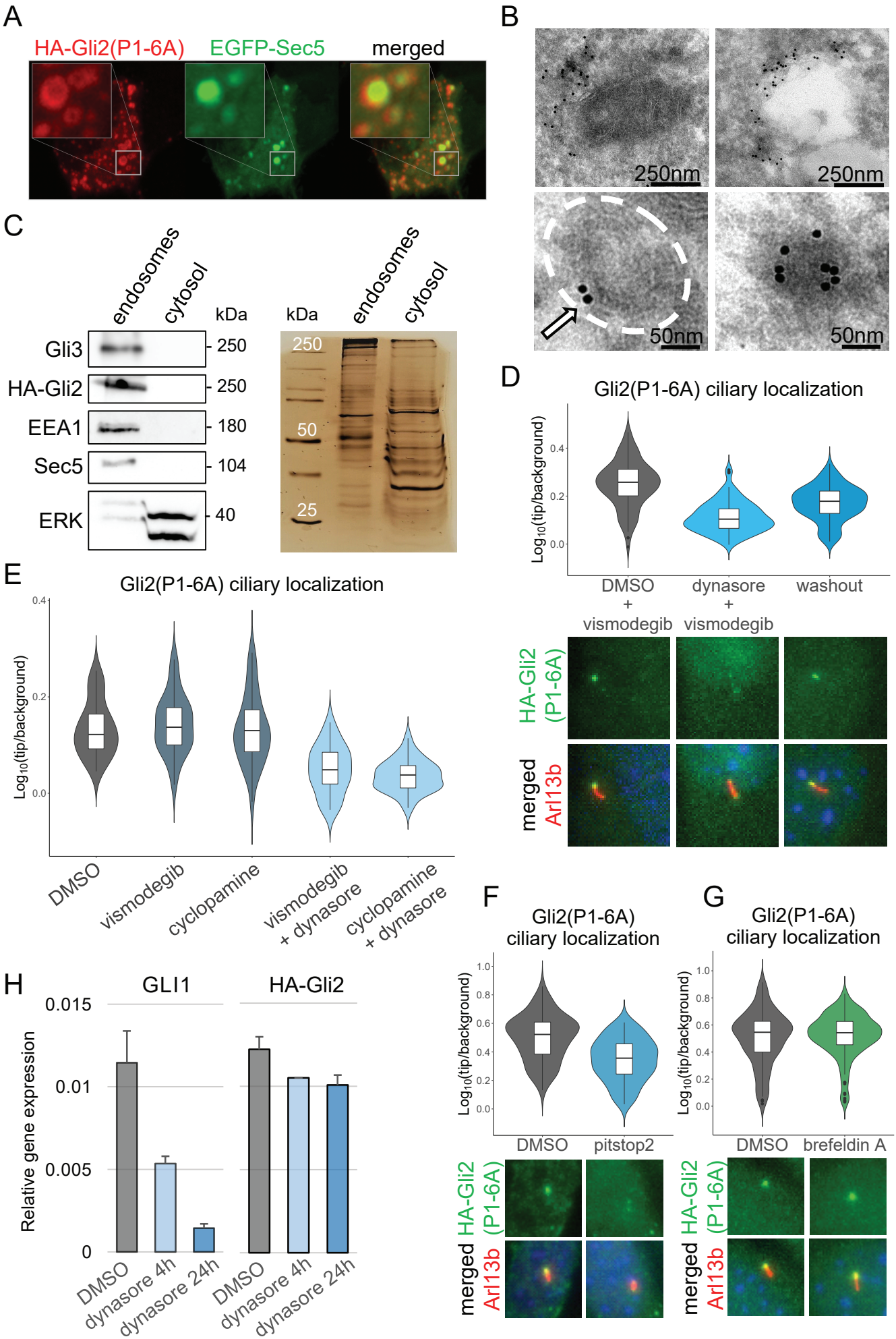
A
HA-Gli2(P1-6A)
EGFP-Sec5
merged
B
250nm
250nm
50nm
50nm
C
endosomes
cytosol
kDa
Gli3
HA-Gli2
EEA1
Sec5
ERK
250
250
180
104
40
kDa
endosomes
cytosol
250
50
25
D
Gli2(P1-6A) ciliary localization
Log10(tip/background)
0.4
0.2
0.0
DMSO + vismodegib
dynasore + vismodegib
washout
HA-Gli2 (P1-6A)
merged
Arl13b
E
Gli2(P1-6A) ciliary localization
Log10(tip/background)
0.4
0.2
0.0
DMSO
vismodegib
cyclopamine
vismodegib + dynasore
cyclopamine + dynasore
F
Gli2(P1-6A) ciliary localization
Log10(tip/background)
1.0
0.8
0.6
0.4
0.2
0.0
DMSO
pitstop2
HA-Gli2 (P1-6A)
merged
Arl13b
G
Gli2(P1-6A) ciliary localization
Log10(tip/background)
1.0
0.8
0.6
0.4
0.2
0.0
DMSO
brefeldin A
HA-Gli2 (P1-6A)
merged
Arl13b
H
GLI1
HA-Gli2
Relative gene expression
0.015
0.01
0.005
0
DMSO
dynasore 4h
dynasore 24h
DMSO
dynasore 4h
dynasore 24h

Fig. 5 Gli2 associates with intracellular vesicles

(A) Airyscan fluorescence imaging of HEK293T cells co-transfected with HA-Gli2(P1-6A) and EGFP-Sec5 stained with anti-HA. Insets show high magnification of the Sec5- and HA-Gli2(P1-6A)-positive vesicle-like structures with Gli2 at the periphery (B) Electron microscopy images of HEK293T cells transfected with EGFP-Gli2(P1-6A) and labeled with immunogold-conjugated anti-GFP. EGFP-positive signal accumulates around vesicle-like structures (C) Cells stably expressing HA-Gli2(P1-6A) were fractionated using the endosome isolation kit and the fractions were resolved using SDS-PAGE. Immunoblot shows HA-Gli2(P1-6A), Gli3, and Sec5 in the endosomal fraction. EEA1 was used as a marker of the endosomes, and ERK was used as a cytosolic fraction marker. The same protein samples were resolved by SDS-PAGE and the gel was silver-stained, showing similar total protein abundance in both fractions. (D) Dynasore impairs Gli2(P1-6A) ciliary localization. Cells were treated with vismodegib in the presence or absence of dynasore for 2h hours and then the drugs were washed out for the indicated times. Relative localization of Gli2(P1-6A) at the cilium tip was measured as in Fig. 3C for n > 80 cilia per group. Student's t-test DMSO+vismodegib vs dynasore+vismodegib p-value < 2.2e-16; dynasore+vismodegib vs washout 1h p-value = 4.25e-05; dynasore+vismodegib vs washout 4h p-value = 6.412e-10. Representative images of Gli2(P1-6A) ciliary localization for each condition are presented below. Arl13b was used as a ciliary marker. (E) Effect of dynasore treatment on Gli2(P1-6A) ciliary accumulation. NIH/3T3 cells with stable expression of HA-Gli2(P1-6A) were treated with dynasore (4h; 40μM) in the presence of Smo inhibitors vismodegib (4h; 3μM) and cyclopamine (4h; 10μM). The Smo inhibitors were used to ensure that the effect of dynasore was not due to its influence on Smo or Ptch trafficking. The Smo inhibitors did not influence Gli2(P1-6A) ciliary accumulation, as expected, and did not prevent dynasore from inhibiting Gli2(P1-6A) localization at the cilium tip. Relative localization of Gli2(P1-6A) at the cilium tip was measured as in Fig. 3C for n > 30 cilia per group. Student's t-test DMSO vs vismodegib p-value = 0.5533; DMSO vs vismodegib+dynasore p-value = 9.047e-08; DMSO vs cyclopamine p-value = 0.8634; DMSO vs cyclopamine+dynasore p-value = 1.708e-10. (F) Effect of pitstop2 treatment on Gli2(P1-6A) ciliary accumulation. Pitstop2 (30μM) was used for 10min and then wash out to avoid its toxicity effect on cell viability. Effect of treatment was observed 30min after washout. Relative localization of Gli2(P1-6A) at the cilium tip was measured as in Fig. 3C for n > 80 cilia per group. Student's t-test DMSO vs pitstop2 30min washout p-value = 2.486e-10. Representative images of Gli2(P1-6A) ciliary localization for each condition are presented below. Arl13b was used as a ciliary marker. (G) Effect of brefeldin A treatment on Gli2(P1-6A) ciliary accumulation. Cells were treated with DMSO or brefeldin A (5μg/ml) for 2h. Relative localization of Gli2(P1-6A) at the cilium tip was measured as in Fig. 3C for n > 140 cilia per group. Student's t-test DMSO vs brefeldin A p-value = 0.4565. Representative images of Gli2(P1-6A) ciliary localization for each condition are presented below. Arl13b was used as a ciliary marker. (H) The relative mRNA expression level of Gli1 (Hh pathway activity marker), and HA-Gli2(P1-6A) after 4h and 24h of dynasore treatment.

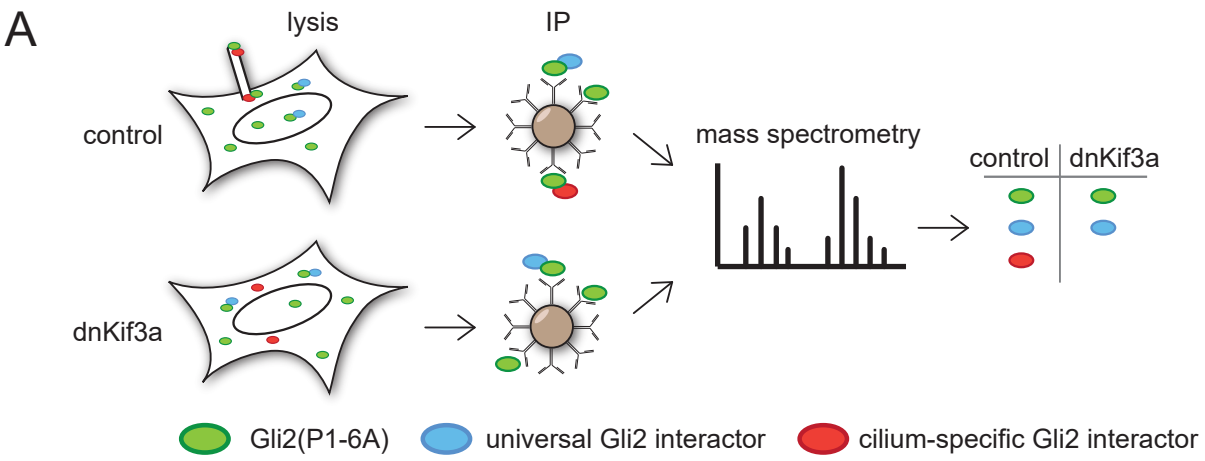

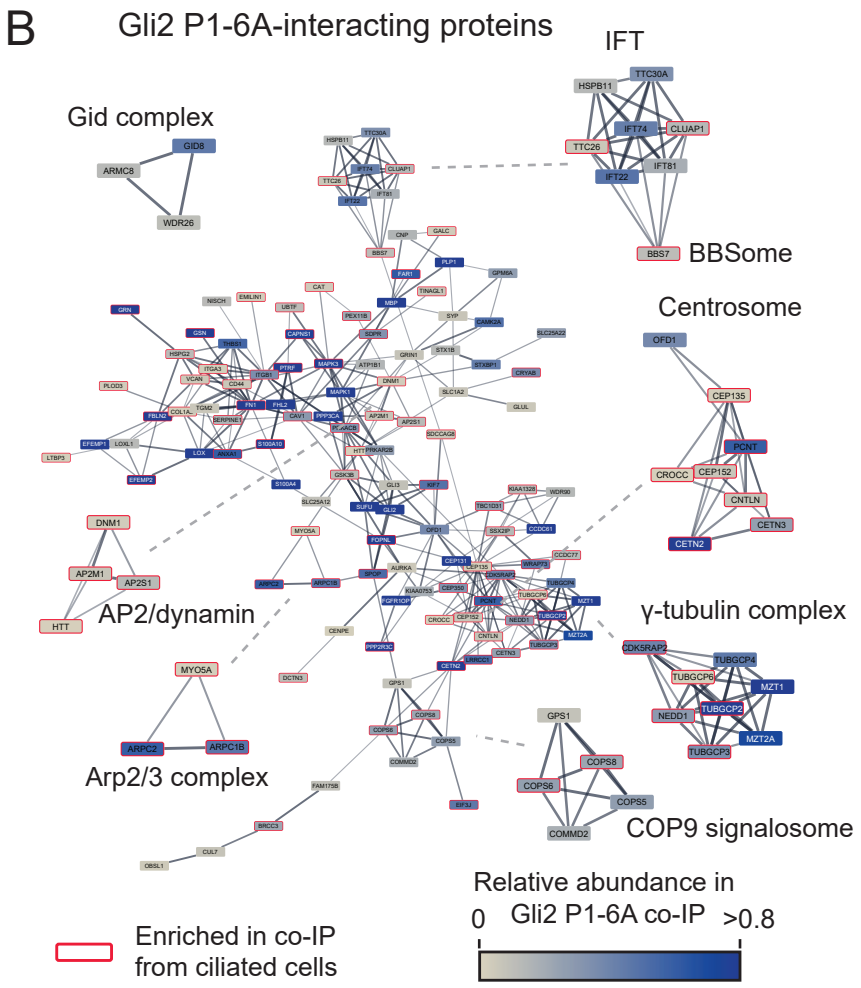

C

Protein	Total enrichment in Gli2 co-IP	Relative co-IP enrichment in ciliated cells	FDR
Arf3	2.00	40%	36%
Arf4	0.95	74%	28%
Rab11b	0.21	100%	17%
Rab14	0.33	100%	21%
Rab18	0.35	75%	12%
Rab3d	0.25	50%	18%
Rab5c	0.26	100%	21%

Fig. 6 Interaction network of Gli2(P1-6A) in ciliated and non-ciliated cells

(A) Schematic representation of the experiment. NIH/3T3 Flp-In cells stably expressing HA-Gli2(P1-6A) and either vector control or Hdominant-negative Kif3a (dnKif3a) were lysed in gentle lysis buffer and the lysates were immunoprecipitated using magnetic beads coated with anti-HA antibodies. Eluted proteins were submitted for mass spectrometric analysis. Common MS-AP contaminants (>10% FDR from the CRAPome database 30) were removed from each dataset (control – ciliated, dnKif3a – non-ciliated) (B) High confidence HA-Gli2(P1-6A) interactors identified by MS were connected into a network using the STRING 106 plugin in Cytoscape. Proteins identified in Gli2(P1-6A) from ciliated and non-ciliated cells were pooled. Shown is the main protein network with the node color representing the approximate relative abundance of the protein in the Gli3 interactome and the edge thickness corresponding to the confidence of connection between proteins in the STRING database. Also shown are highly interconnected sub-networks identified using MCODE clustering, which typically corresponds to protein complexes or multiprotein functional units. Proteins that were identified predominantly in the ciliated cells are marked with red borders (C) Small GTPases identified in Gli2(P1-6A) co-IP/MS experiments are shown, with their relative enrichment scores, relative enrichment in ciliated vs non-ciliated cell co-IP samples, and FDR scores based on the CRAPome database.

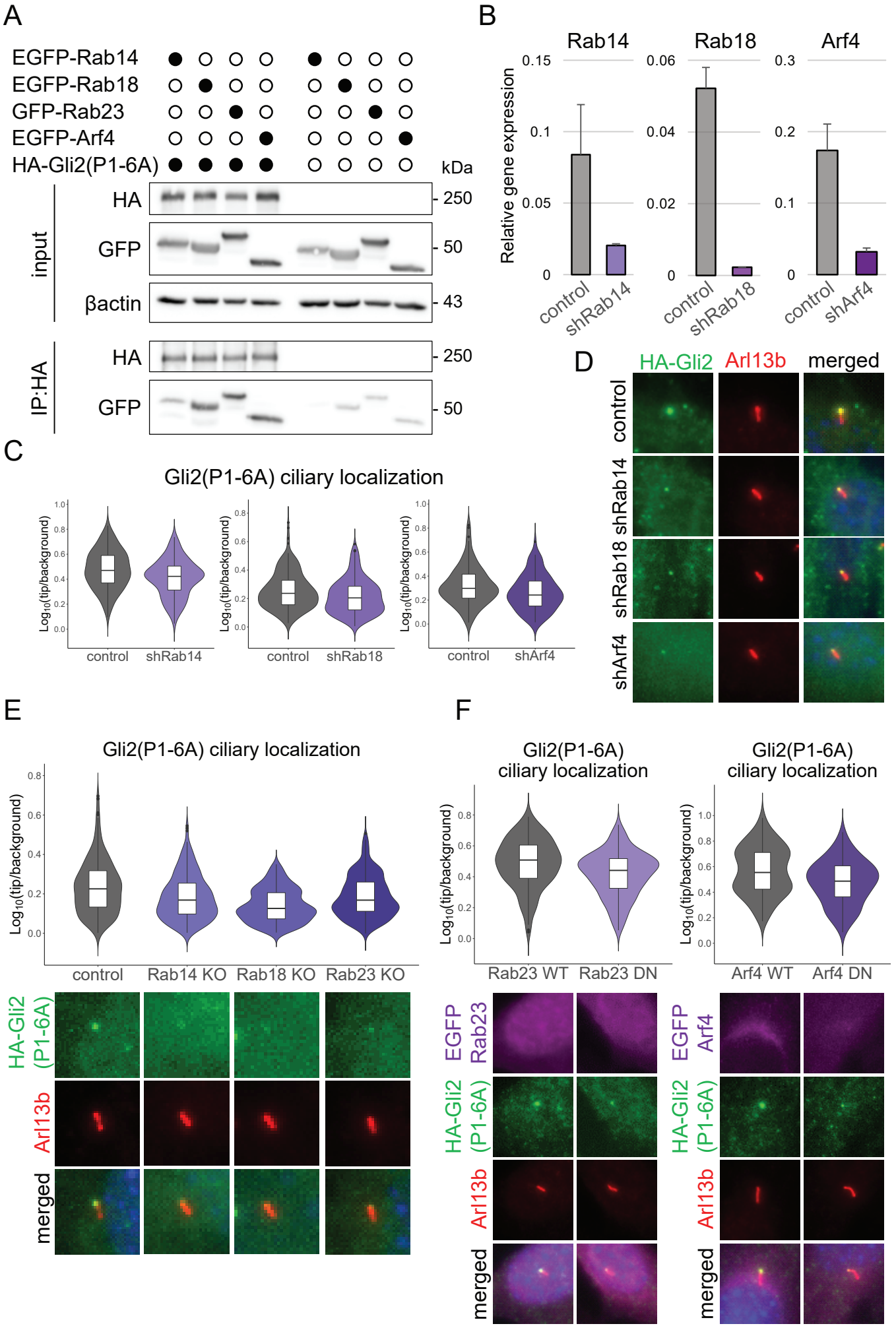
A
EGFP-Rab14
EGFP-Rab18
GFP-Rab23
EGFP-Arf4
HA-Gli2(P1-6A)
kDa
input
HA
GFP
βactin
250
50
43
IP:HA
HA
GFP
250
50
B
Rab14
Rab18
Arf4
Relative gene expression
control
shRab14
shRab18
shArf4
C
Gli2(P1-6A) ciliary localization
Log10(tip/background)
control
shRab14
shRab18
shArf4
D
HA-Gli2
Arl13b
merged
control
shRab14
shRab18
shArf4
E
Gli2(P1-6A) ciliary localization
Log10(tip/background)
control
Rab14 KO
Rab18 KO
Rab23 KO
HA-Gli2 (P1-6A)
Arl13b
merged
F
Gli2(P1-6A) ciliary localization
Log10(tip/background)
Rab23 WT
Rab23 DN
Gli2(P1-6A) ciliary localization
Log10(tip/background)
Arf4 WT
Arf4 DN
EGFP Rab23
HA-Gli2 (P1-6A)
Arl13b
merged
EGFP Arf4
HA-Gli2 (P1-6A)
Arl13b
merged

Fig. 7 Rab14, Rab18, Rab23, and Arf4 mediate Gli2 ciliary trafficking into primary cilium

(A) Co-immunoprecipitation of EGFP tagged Rab and Arf proteins with HA-Gli2(P1-6A). HEK293T cells were co-transfected with the indicated constructs and co-IP was performed as in Fig. 2C (B) Knockdown efficiency of Rab14, Rab18, and Arf4 using shRNA. Cells were transduced with viral constructs encoding the indicated shRNAs and mRNA expression of their target genes was measured by qRT-PCR. Control cells were transduced with the shRNA against luciferase (C) Effect of Rab14, Rab18, and Arf4 shRNA knockdown on relative Gli2(P1-6A) ciliary localization. Relative localization of Gli2(P1-6A) at the cilium tip was measured as in Fig. 3C for n > 100 cilia per group. Student's t-test control vs shRNA Rab14 p-value = 0.00018; control vs shRNA Rab18 p-value = 0.00027; control vs shRNA Arf4 p-value = 0.0081 (D) Representative images of HA-Gli2(P1-6A) localization in cilia of cells with the knockdown of Rab14, Rab18 and Arf4. Cells were transduced as in B. Arl13B was used as a ciliary marker (E) Effect of CRISPR-Cas9-mediated knockout of Rab14, Rab18, and Rab23 on Gli2(P1-6A) ciliary localization. Cells stably expressing both HA-Gli2(P1-6A) and Cas9 were transduced with viral constructs encoding the indicated sgRNAs. Control cells were transduced with the empty pLentiGuide-puro vector. Relative localization of Gli2(P1-6A) at the cilium tip was measured as in Fig. 3C for n > 280 cilia per group. Student's t-test control vs Rab14 edit p-value = 1.1e-06; control vs Rab18 edit p-value < 2.2e-16; control vs Rab23 edit p-value = 3.4e-07. Representative images of Gli2(P1-6A) ciliary localization for each condition are presented below. Arl13b was used as a ciliary marker. (F) Effect of inducible expression of dominant-negative (DN) forms of Rab23 and Arf4 on Gli2(P1-6A) ciliary localization. Relative localization of Gli2(P1-6A) at the cilium tip was measured as in Fig. 3C for n > 100 cilia per group. Student's t-test Rab23 WT vs DN p-value = 2.2e-05; Arf4 WT vs DN p-value = 0.00031. Representative images of Gli2(P1-6A) ciliary localization for each condition are presented below. Arl13b was used as a ciliary marker.

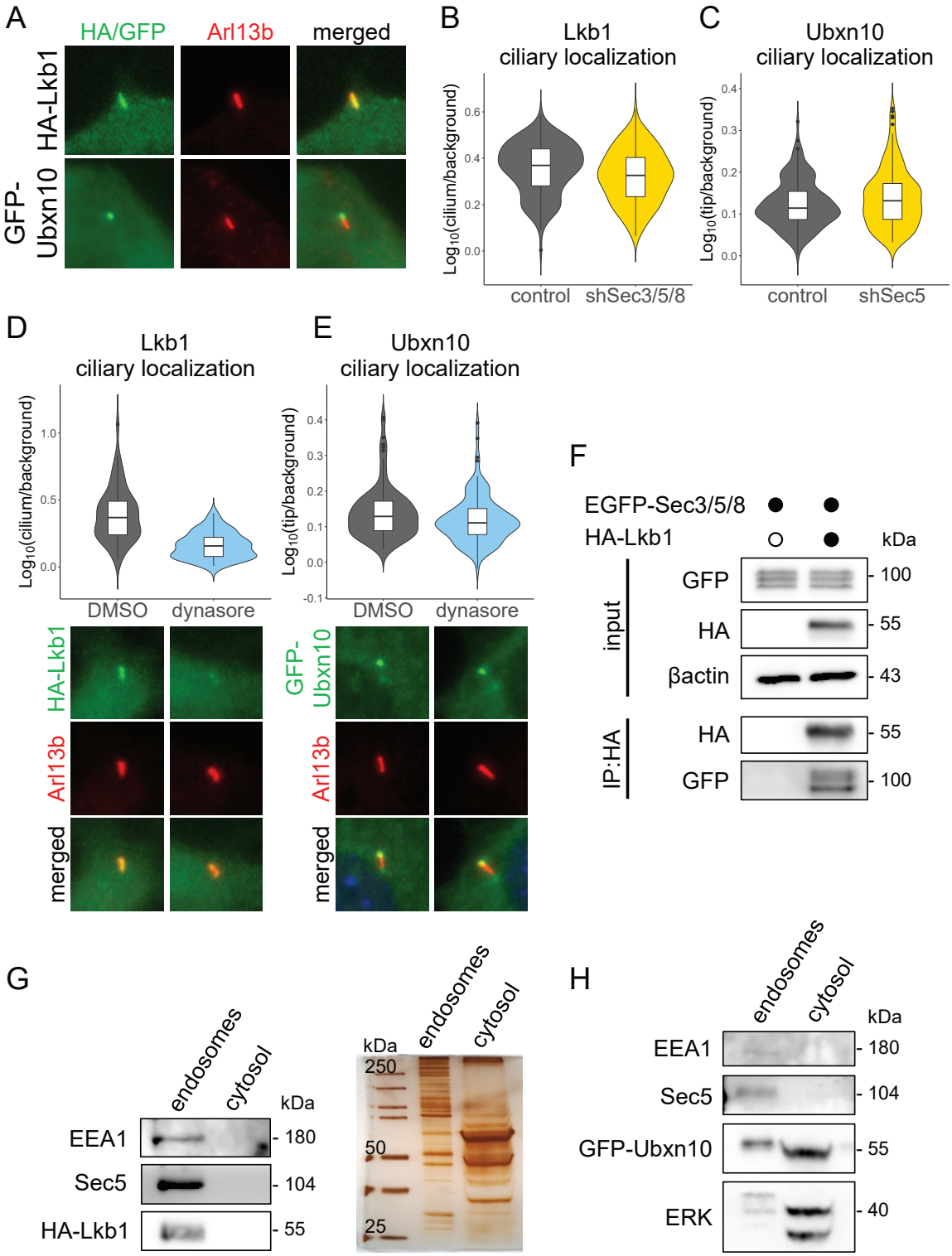

Fig. 8 The trafficking of Lkb1, but not Ubxn10, depends on endocytosis and the exocyst

(A) Ciliary localization of Lkb1 and Ubxn10 in NIH/3T3 cells. Cells were transfected and stained with the indicated antibodies. Arl13b was used as a ciliary marker. (B) Effect of Sec3/5/8 shRNA knockdown on Lkb1 ciliary localization. Cells were transduced as in Fig 3A. Relative localization of Lkb1 at the cilium tip was measured as in Fig. 3C for n > 70 cilia per group. Student's t-test control vs shSec3/5/8 p-value = p-value = 0.003 (C) Effect of Sec5 shRNA knockdown on relative Ubxn10 ciliary localization. Cells were transduced as in Fig 3A. Relative localization of Ubxn10 at the cilium tip was measured as in Fig. 3C for n > 160 cilia per group. Student's t-test control vs shSec5 p-value = 0.037 (D) Effect of dynasore treatment on Lkb1 ciliary accumulation. NIH/3T3 cells with stable expression of HA-Lkb1 were treated with DMSO and dynasore (4h; 40μM). Relative localization of Lkb1 at the cilium was measured for n > 50 cells per group. Student's t-test p-value = 2.3e-11. Representative images are presented below. (E) Effect of dynasore treatment on Ubxn10 ciliary accumulation. Cells were treated as in B and relative localization was measured for n > 100 cells per group. Student's t-test DMSO vs dynasore 4h p-value = 0.05. Representative images are presented below. (F) Co-immunoprecipitation of EGFP tagged Sec3/5/8 proteins with HA-Lkb1 in HEK293T cells co-transfected with the indicated constructs (G) Cells stably expressing HA-Lkb1 were fractionated using the endosome isolation kit and the fractions were resolved using SDS-PAGE. Immunoblot shows Lkb1 in the endosomal fraction. EEA1 was used as a marker of the endosomes. Silver-stained gel of the same samples shows similar total protein abundance in both fractions. (H) Fractionation of stably expressed GFP-Ubxn10 cells as in G. Immunoblot shows Ubxn10 mainly in the cytosolic fraction. ERK was used as a cytosolic fraction marker.

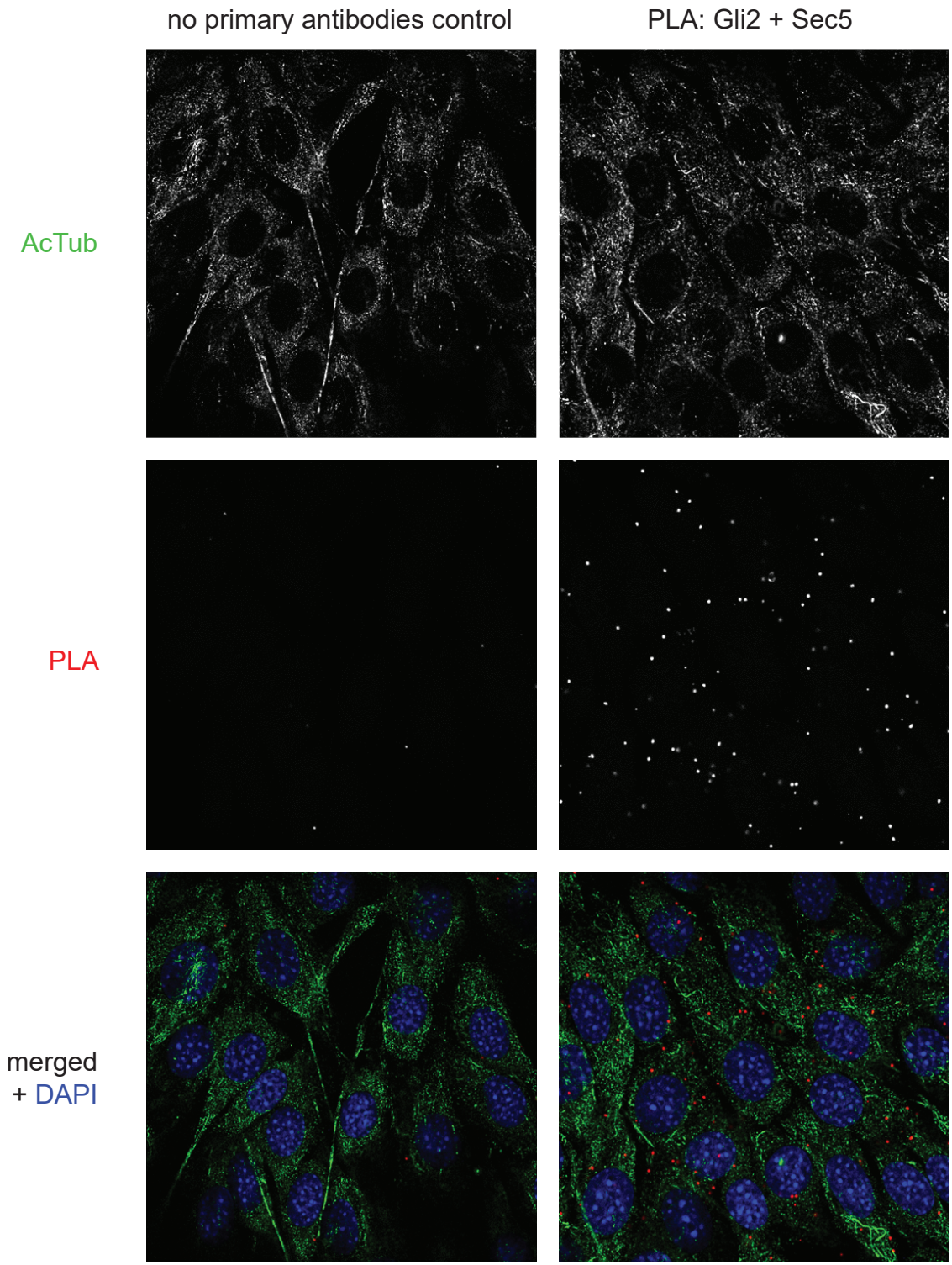

Figure S1. Proximity Ligation Assay with anti-Gli2 and anti-Sec5 antibodies in NIH/3T3 mouse fibroblasts. Sites of interaction are marked in red. Cilia were stained with anti-acetylated tubulin (green), and nuclei with DAPI (blue). Larger areas with multiple cells are shown compared to Fig. 2B.

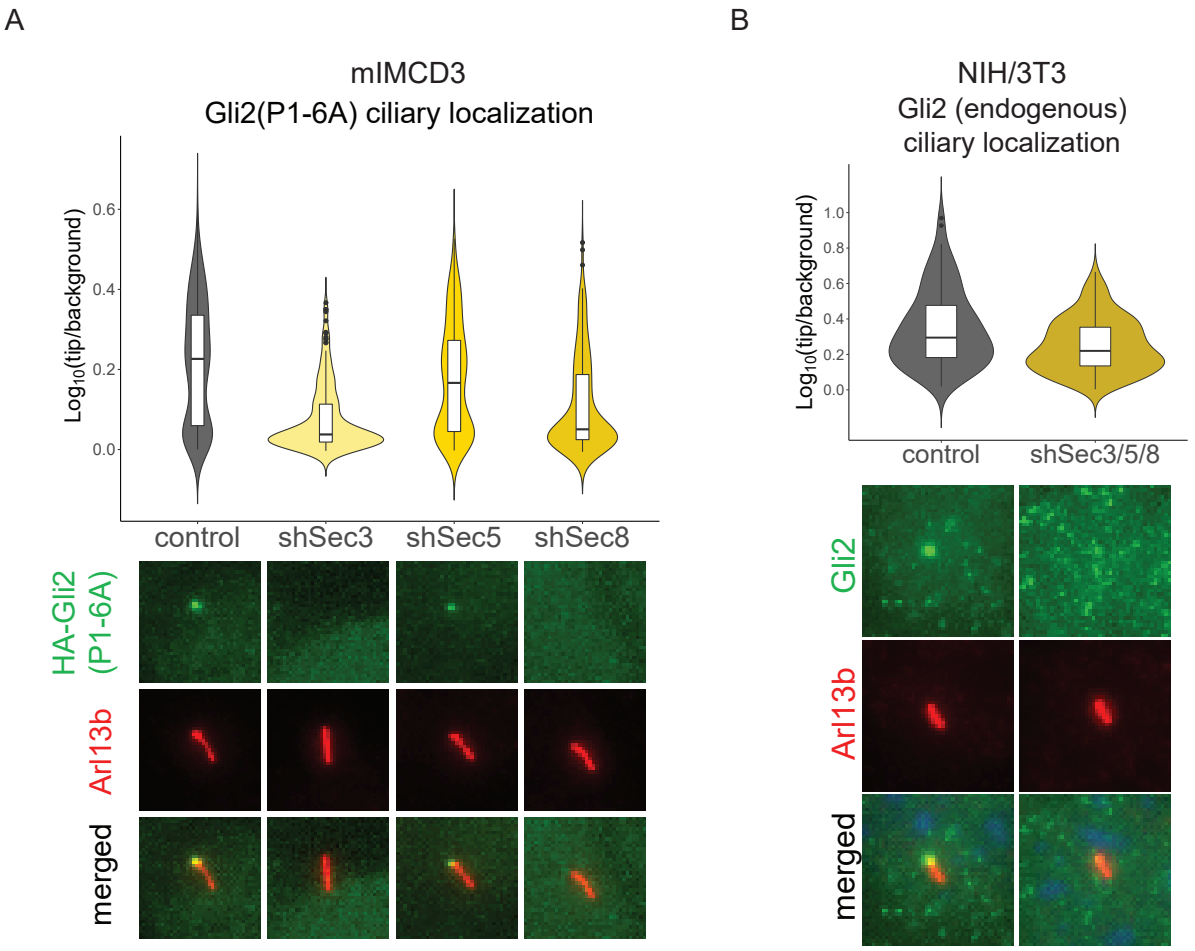

Figure S2. A. Effect of Sec3/5/8 shRNA knockdown on relative Gli2(P1-6) ciliary localization in mIMCD3 cells with stable expression of Gli2(P1-6A). Cells were transduced as in Fig 3A. Control cells were transduced with shRNA against luciferase. Relative localization of Gli2(P1-6A) at the cilium tip was measured as in Fig. 3C for n > 240 cilia per group. Student's t-test control vs shSec3 p-value < 2.2e-16; control vs shSec5 p-value = 0.001585; control vs shSec8 p-value < 2.2e-16. B. Relative localization at the cilium tip of endogenous Gli2 in NIH/3T3 cells with shRNA knockdown of Sec3, Sec5, and Sec8 and treated for 24h with SAG agonist. Results are presented as violin plots of log10-transformed ratios of fluorescence intensity of anti-HA staining at cilia tips to the intensity in the surrounding background. Cilia per variant n > 90. Student's t-test analysis control-shSec3/5/8 p-value = 0.0026. Representative images of Gli2 ciliary localization for each condition are presented below. Arl13b was used as a ciliary marker.

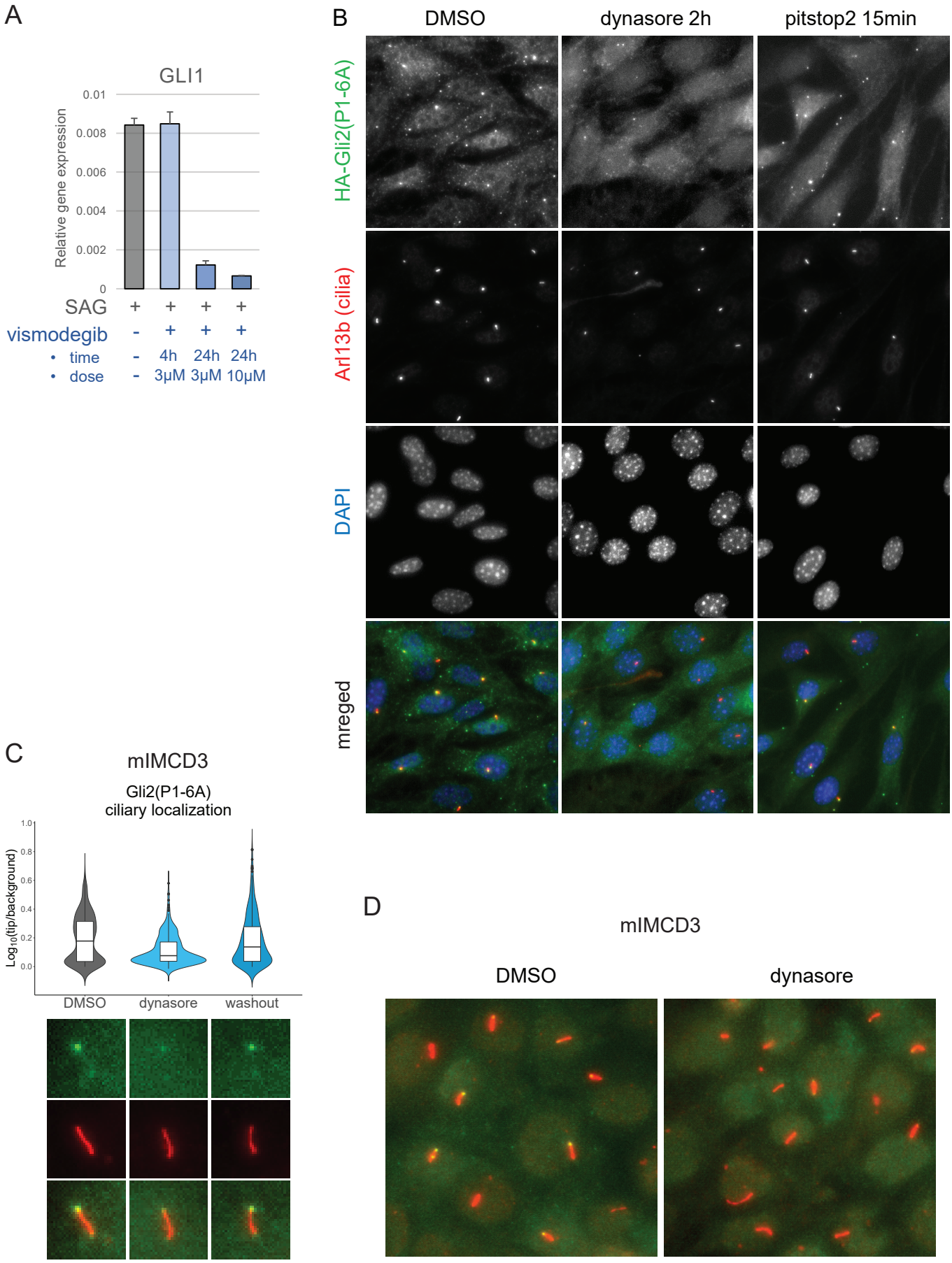

Figure S3. A. The relative mRNA expression level of Gli1 (Hh pathway activity marker) after indicated dose and time of vismogedib treatment. B. Low magnification images of NIH/3T3 cells treated with dynasore or pitstop2 (see Fig. 5D and Fig. 5F). Cell morphology appears normal with no apparent toxicity (cell rounding or detaching, chromatin condensing or fragmenting). C. mIMCD3 Flp-in cells with stable expression of HA-Gli2(P1-6A) were treated with dynasore (2h; 40μM) and then the drug was washed out for 2h. Relative localization of Gli2(P1-6A) at the cilium tip was measured as in Fig. 3C for n > 300 cilia per group. Student's t-test DMSO vs dynasore p-value = 2.433e-13; dynasore vs washout p-value = 2.698e-13; DMSO vs washout p-value = 0.6375. D. Dynasore did not disrupt mIMCD3 cells after 2h treatment. Cell morphology and cilia morphology remain unchanged.

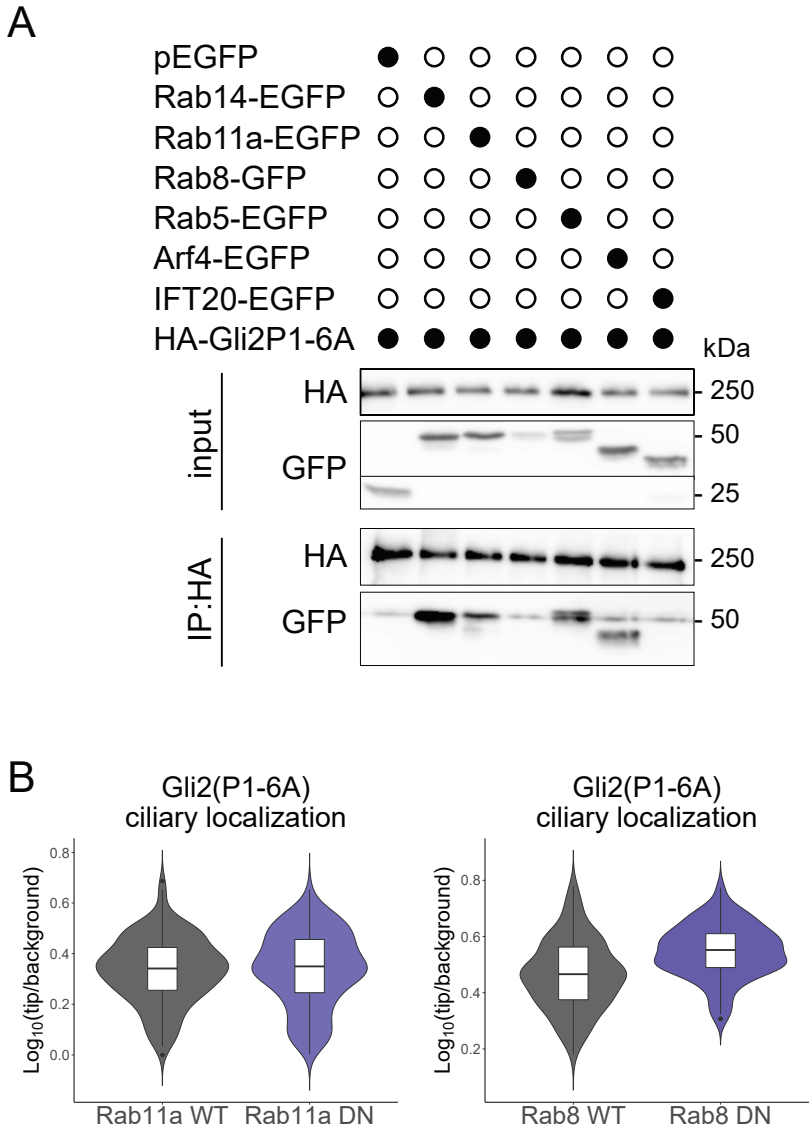

Figure S4 (A) Co-immunoprecipitation of EGFP tagged Rab, Arf, and IFT proteins with HA-Gli2(P1-6A). HEK293T cells were co-transfected with the indicated constructs and co-IP was performed using the HA beads. (B) Effect of inducible expression of dominant-negative (DN) forms of Rab8 and Rab11a on Gli2(P1-6A) ciliary localization. Relative localization of Gli2(P1-6A) at the cilium tip was measured as in Fig. 3C for n > 120 cilia per group. Student's t-test Rab11a WT vs DN p-value = 0.70; Rab8 WT vs DN p-value = 2.5e-08.

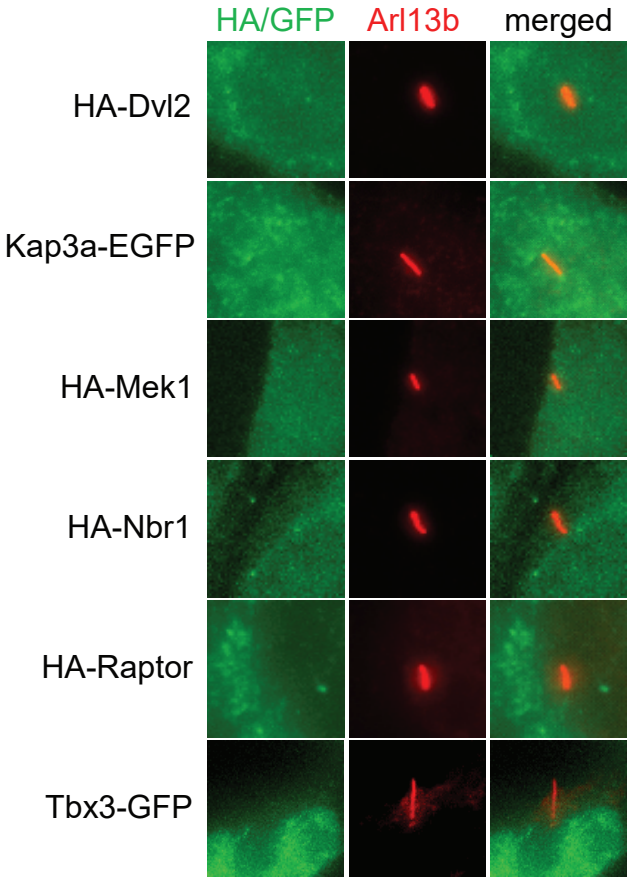

Figure S5. Ciliary localization of different putative ciliary proteins we tested in NIH/3T3 cells. Cells were transfected with indicated proteins tagged with HA or GFP and then we observed their ciliary localization. Arl13b was used as a ciliary marker.